Ocean Sci., 8, 497–523, 2012
www.ocean-sci.net/8/497/2012/
doi:10.5194/os-8-497-2012

Ocean Science

Atlantic transport variability at 25° N in six hydrographic sections

C. P. Atkinson[1,*], **H. L. Bryden**[1], **S. A. Cunningham**[1], **and B. A. King**[1]

[1]National Oceanography Centre, European Way, Southampton, SO14 3ZH, UK
[*]now at: Met Office Hadley Centre, FitzRoy Road, Exeter, Devon, EX1 3PB, UK

Correspondence to: C. P. Atkinson (chris.atkinson@metoffice.gov.uk)

Received: 19 December 2011 – Published in Ocean Sci. Discuss.: 16 January 2012
Revised: 23 April 2012 – Accepted: 22 May 2012 – Published: 19 July 2012

Abstract. In January and February 2010, a sixth transatlantic hydrographic section was completed across 25° N, extending the hydrographic record at this latitude to over half a century. In combination with continuous transport measurements made since 2004 at 26.5° N by the Rapid-WATCH project, we reassess transport variability in the 25° N hydrographic record. Past studies of transport variability at this latitude have assumed transport estimates from each hydrographic section to represent annual average conditions. In this study the uncertainty in this assumption is assessed through use of Rapid-WATCH observations to quantify sub-seasonal and seasonal transport variability. Whilst in the upper-ocean no significant interannual or decadal transport variability are identified in the hydrographic record, in the deep ocean transport variability in both depth and potential temperature classes suggests some interannual or decadal variability may have occurred. This is particularly striking in the lower North Atlantic Deep Water where southward transports prior to 1998 were greater than recent transports by several Sverdrups. Whilst a cooling and freshening of Denmark Straits Overflow Water has occurred which is coincident with these transport changes, these water mass changes appear to be density compensated. Transport changes are the result of changing velocity shear in the vicinity of the Deep Western Boundary Current.

1 Introduction

In January and February 2010, a sixth hydrographic section was completed across 25° N in the Atlantic Ocean, extending the decadal timeseries of hydrographic measurements available at this latitude. Previous hydrographic sections were carried out in 1957 as part of the International Geophysical Year (Fuglister, 1960), in 1981 (Roemmich and Wunsch, 1985), in 1992 and 1998 during the World Ocean Circulation Experiment (Parrilla et al., 1994; Baringer and Molinari, 1999), and in 2004 (Bryden et al., 2005b). Despite the seemingly sparse nature of the observations, the oceanographic section across 25° N represents one of the best observed regions of the world oceans and offers an excellent opportunity to investigate large-scale decadal changes in ocean state.

When comparing hydrographic "snapshots" of the ocean, a classic problem associated with the interpretation of decadal changes is the possible aliasing of changes in the ocean state at shorter timescales. An absence of continuous in situ measurements has made this issue difficult to address and in the past it has mostly been dealt with indirectly using estimates of the magnitude and nature of high frequency variability. Since April 2004 the Rapid-WATCH project (Rapid climate change – Will the Atlantic Thermohaline Circulation Halt) has provided continuous observations of Atlantic transport variability at 26.5° N. This has revealed surprisingly large transport variability on sub-seasonal and seasonal timescales (Cunningham et al., 2007; Kanzow et al., 2010) and has raised questions over the significance of longer term trends in Atlantic transport reported in earlier 25° N hydrographic sections that suggested a weakening of the Atlantic Meridional Overturning Circulation (AMOC) (Bryden et al., 2005b).

Understanding AMOC variability is an important challenge for the scientific community. The AMOC is a fundamental part of Earth's climate system, transporting large amounts of heat into the high northern latitudes. Model studies predict a substantial weakening of the AMOC in response to anthropogenic related changes in high latitude buoyancy flux (IPCC, 2007) and a total shutdown of the AMOC would have profound implications for the climate of northwest Europe (Vellinga and Wood, 2002). Due to the sparse nature

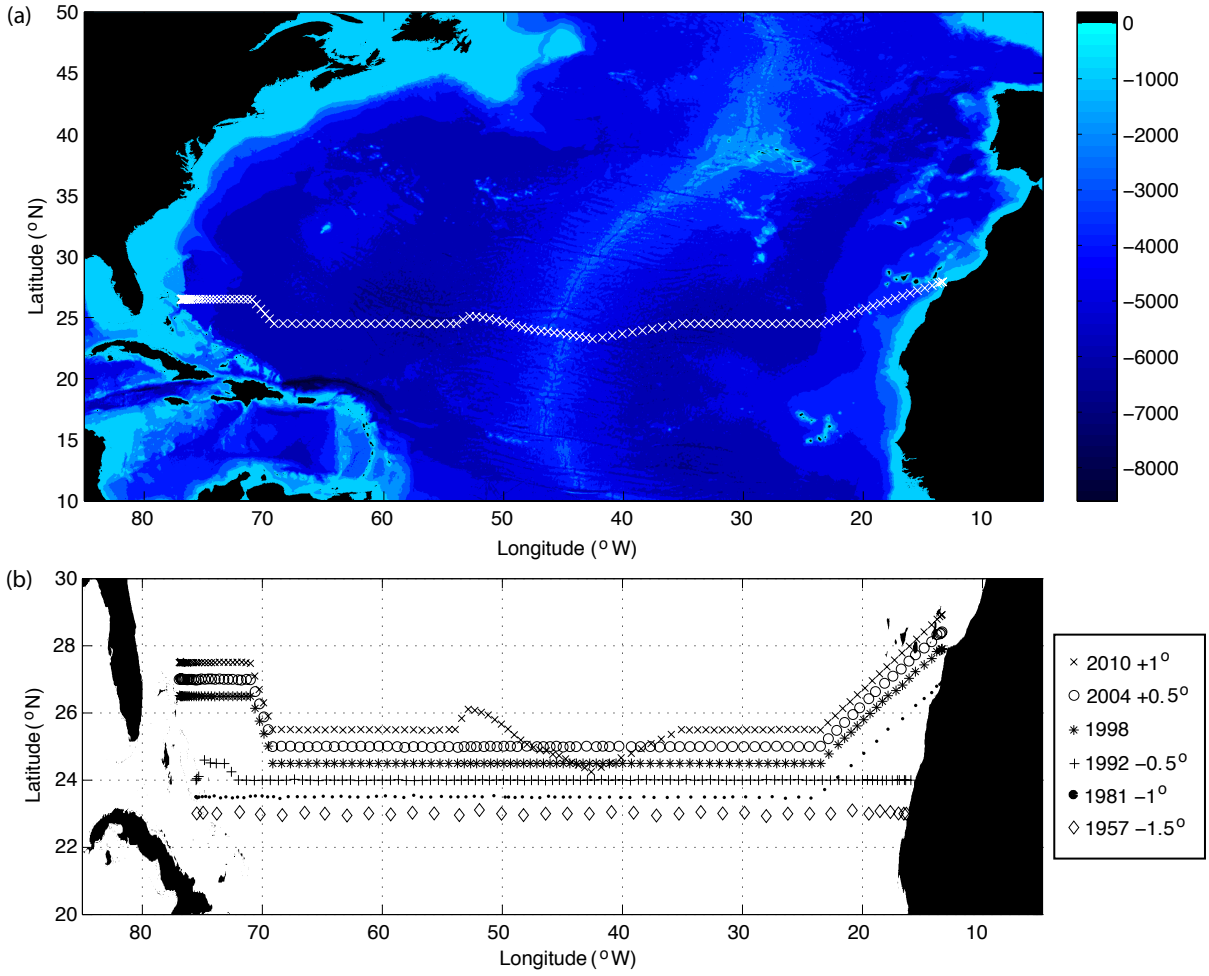

Fig. 1. (a) Bathymetric map (Smith and Sandwell, 1997) of the subtropical North Atlantic with mid-ocean CTD stations from the 2010 hydrographic cruise overlaid **(b)** CTD stations for the six hydrographic cruises completed across 25° N, note that cruise tracks are offset by 0.5° increments for clarity with 1998 at the correct latitude.

of AMOC observations presently available, the extent, magnitude and origin of AMOC variability at interannual to decadal timescale are still uncertain and model studies cannot yet be validated. Whilst targeted observational programmes such as Rapid-WATCH are beginning to address this lack of observations, extracting further understanding on variability of the AMOC and its components from existing observations is also extremely useful.

Motivated by the completion of the 2010 hydrographic section and the availability of Rapid-WATCH observations, this study revisits the question of transport variability in the hydrographic record at 25° N. Five years of Rapid-WATCH observations are used to quantify the magnitude of sub-seasonal and seasonal transport variability at this latitude to assess the assumption that each hydrographic section represents annual average conditions (Bryden et al., 2005b). We then examine whether any significant interannual or longer term changes have been observed in the six hydrographic sections which is outside the range of shorter term variability in the Rapid-WATCH observations.

This study largely concentrates on transport variability in the Upper and Lower North Atlantic Deep Waters (UNADW and LNADW) which together form the lower limb (deeper than approximately 1000 m) of the AMOC. In past discussions of transport variability at 25° N the deep waters have received somewhat less attention than the waters of the upper limb of the AMOC. However, short-term transport variability in the deep ocean is shown here to be reduced relative to transport variability in the upper ocean such that longer term transport changes are more likely to be discerned at depth. Furthermore, variability in the formation rate of NADW in the Labrador and Nordic Seas is thought to be an important forcing of interannual and decadal AMOC variability, as observed in model studies (e.g. Eden and Willebrand, 2001; Boening et al., 2006; Stouffer et al., 2006; Biastoch et al., 2008; Koehl and Stammer, 2008).

2 Data and methods

2.1 Hydrographic data

Repeat occupations of the 25° N transatlantic section were made in October 1957, August–September 1981, July–August 1992, January–February 1998, April–May 2004 and January–February 2010. The cruise tracks for each of these sections and a bathymetric map of the subtropical Atlantic is shown in Fig. 1 (note that the cruise tracks are offset by 0.5° latitude for clarity). In the mid-ocean, all sections follow 24.5° N, though for the 2010 section a distinct kink is seen in the cruise track over the Mid Atlantic Ridge (MAR) where the main trench of the Kane Fracture Zone was followed. In the east, the 1981, 1998, 2004 and 2010 sections deviate north toward 28° N approaching the African coastline due to diplomatic clearance issues. In the west the 1998, 2004 and 2010 sections meet the Bahamas at 26.5° N so the section transports can be closed using cable measurements in the Florida Straits. The sections from 1981 onwards also comprise a short transect across the Florida Straits at 26.5° N. All sections except 1957 are eddy resolving and have closer station spacing near the western and eastern boundaries and over the rugged topography of the MAR.

The 1981 through 2010 sections consist of between 90 and 122 vertical temperature, salinity and oxygen profiles obtained from CTD observations which are effectively continuous throughout the water column. The 1957 section comprises 38 profiles using discrete Nansen bottle sampling for temperature, salinity and oxygen at approximately 25 depths from top to bottom. Whilst salinity measurements for the 1957 dataset were made using modern conductivity techniques, concern exists over the accuracy of these salinities which may be biased high by 0.004 to 0.006 (Bryden et al., 1996). Calculations of decadal changes in transport and water mass properties that use the 1957 data must, therefore, be treated with caution. All hydrographic datasets are interpolated onto 20 dbar levels, the working vertical resolution of this study.

2.2 Rapid-WATCH data

The Rapid-WATCH data used in this study comprises five years of continuous observations of the strength of the AMOC. These span the period April 2004 to April 2009 and constitute the longest record available at the time of analysis. Data were downloaded from http://www.noc.soton.ac.uk/rapidmoc. The Rapid-WATCH array (shown in Fig. 2) combines Ekman transport calculated from satellite wind stress, Florida Current cable measurements of Gulf Stream transport, ADCP and moored current meter measurements on the Bahamian continental shelf, and zonally integrated mid-ocean geostrophic transports calculated using moored temperature and salinity sensors located at the basin margins and the Mid-Atlantic ridge. Together these observations allow total transport across 26.5° N to be measured down to 5000 m depth (Kanzow et al., 2010). Below 5000 m, transport variability is not directly observed and is set to a time invariant value of 2.1 Sv representing northward flow of Antarctic Bottom Water based on estimation from the pre-2010 hydrographic sections (Bryden et al., 2005b). The array design is, however, continuously evolving and moorings MAR0 and WB6 (Fig. 2) form part of recent array designs (since Spring 2007) intended to directly measure AABW variability. This is not included here as the effective deep record was only 6 months long at the time of analysis. Frajka-Williams et al. (2011) report these measurements of deep AABW variability. For each twice-daily observation, section-wide mass balance is ensured through use of a compensation velocity which is applied uniformly across the section and removes any imbalance between array components (this is applied as a reference velocity adjustment to the mid-ocean geostrophic transports). The assumption of mass balance has been demonstrated to hold at periods longer than 10 days (Kanzow et al., 2007), thus, Rapid-WATCH timeseries are available as 10-day low-pass filtered values. Final transport measurements for each of the array components are available on a 20 decibar grid.

In addition to transport profiles, Rapid-WATCH also makes calibrated temperature and salinity profiles available for some of the taller deep-water moorings shown in Fig. 2 (these are WB2, WB3, WB5, MAR1 and MAR2; note that WB4 sits within the Deep Western Boundary Current (DWBC), but has suffered significant instrument loss and failure over deployment periods from 2004–2008 whilst EB1 provides redundancy for the short moorings at the eastern margin). At the ocean margins, mooring data are merged together vertically to provide full depth profiles of hydrographic properties which are used in the calculation of mid-ocean transports. At the African margin a gentle continental slope means it is necessary to merge together a series of short vertical mooring profiles to construct a full depth profile and minimise bottom triangles. At the western margin, WB2 data shallower than 4000 m is merged with data from WB3 at greater depth. Merging of profile data is done by the Rapid-WATCH team. All profile data are freely available from http://www.noc.soton.ac.uk/rapidmoc. Temperature and salinity measurements for individual moored instruments are calibrated for offsets and linear trends using shipboard CTD dips which are completed before deployment and after recovery of each instrument. Instruments are typically deployed for a year at a time. The timeseries instrument records are 2-day low-pass filtered to remove tidal and inertial variability, sampled at 12 hourly resolution and interpolated onto a 20 decibar grid prior to use in transport calculations. On each mooring, instruments are spaced more closely in the upper ocean where vertical property gradients are greater (typically 50–100 m in the pycnocline, 200–500 m in the deep ocean).

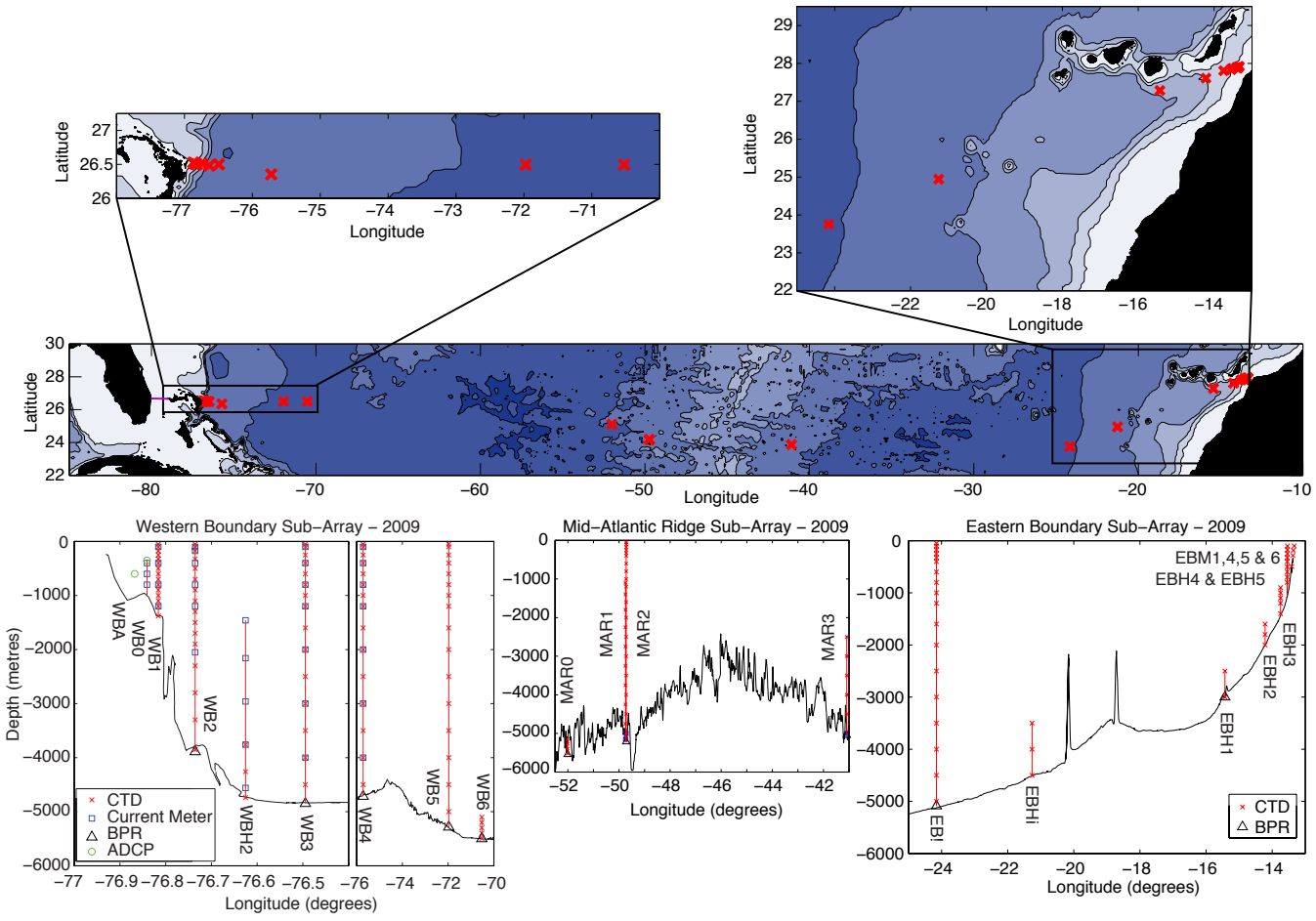

Fig. 2. Map of the Rapid-WATCH moored array in Autumn 2009 (the location of the Florida Straits cable is also shown in purple). Red crosses correspond to mooring locations, enlargements of the western and eastern boundary arrays are shown. Schematic figures of the moorings are given below, including instrumentation, topography and mooring nomenclature. Sub-figures courtesy of Darren Rayner (National Oceanography Centre, Southampton, UK).

2.3 Calculation of hydrographic transports

2.3.1 Method

For each of the hydrographic sections, transport across 25° N is calculated using a similar approach to Longworth (2007), much of which is reiterated below. This in turn broadly follows the method of Hall and Bryden (1982) who calculate the mid-ocean geostrophic flow field based on mass balance constraints using annual average Ekman and Florida Straits components (from wind stress climatologies and Florida Straits cable measurements). Calculating mid-ocean transport using this approach assumes that each one-time hydrographic section represents annual mean conditions i.e., that baroclinic flow structure in the sub-tropics does not respond to wind or thermal forcing on sub-annual timescales (e.g. Jayne and Marotzke, 2001) and that at this timescale any barotropic response to external forcing occurs uniformly across the section. Given the large sub-seasonal and seasonal mid-ocean transport variability recently resolved by the Rapid-WATCH array at this latitude (Cunningham et al., 2007; Kanzow et al., 2010), these assumptions now look uncertain and the changes between hydrographic sections cannot necessarily be interpreted as interannual and decadal variability. The availability of property observations (e.g., salinity and temperature) along the 25° N section can, however, assist in the identification and attribution of the variability being observed.

For each hydrographic section, mid-ocean transports are calculated assuming the observed density structure is geostrophically balanced by the velocity field except in an ageostrophic surface boundary layer forced directly by the wind stress. Geostrophic velocity shear relative to some reference level is computed for each station pair down to the

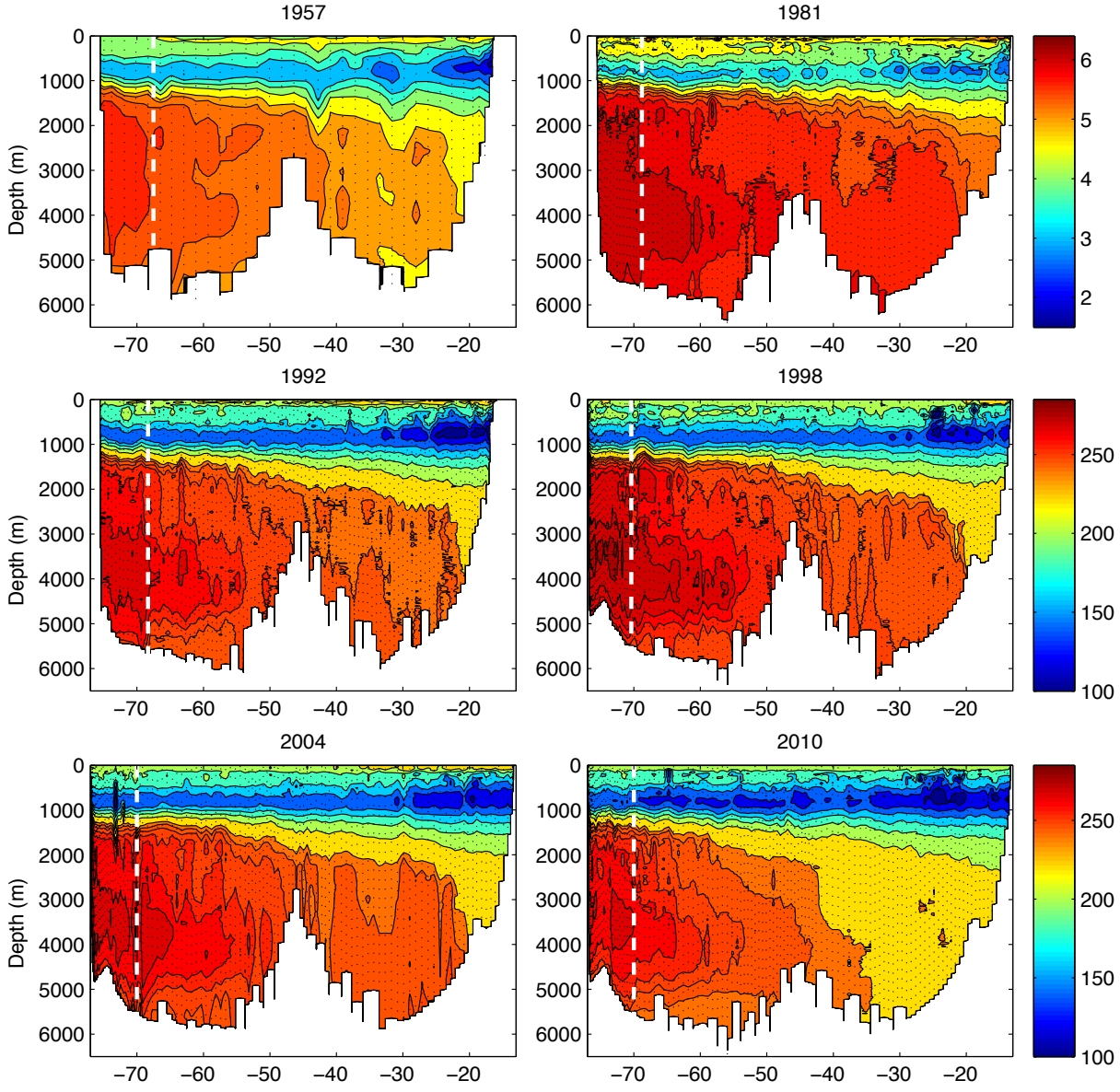

Fig. 3. Oxygen concentrations across 25° N for the 1957, 1981, 1992, 1998, 2004 and 2010 hydrographic sections (following Longworth, 2007). Oxygen concentrations for the 1957 and 1981 sections (top) are given in $\mathrm{ml\,l^{-1}}$ and share the same colour scale; contour intervals change from $0.5\,\mathrm{ml\,l^{-1}}$ to $0.2\,\mathrm{ml\,l^{-1}}$ at concentrations above $5\,\mathrm{ml\,l^{-1}}$. Oxygen concentrations for the later sections are given in $\mu\mathrm{mol\,kg^{-1}}$ and share the same colour scale; contour intervals change from $20\,\mu\mathrm{mol\,kg^{-1}}$ to $5\,\mu\mathrm{mol\,kg^{-1}}$ above $240\,\mu\mathrm{mol\,kg^{-1}}$. The transition between the western boundary region and mid-ocean is shown as a white dotted line, station positions are shown as black dotted lines.

deepest common pressure using:

$$(v - v_{\mathrm{r}}) = \frac{1}{f\,\Delta x}\left(\int_{P_{\mathrm{r}}}^{P} \delta_1\,dp - \int_{P_{\mathrm{r}}}^{P} \delta_2\,dp\right), \qquad (1)$$

where v is the average geostrophic velocity ($\mathrm{m\,s^{-1}}$) between two hydrographic stations 1 and 2 at pressure P (Pascals) relative to pressure P_{r}, δ is the specific volume anomaly ($\mathrm{m^3\,kg^{-1}}$) integrated between pressure levels P and P_{r}, Δx is the horizontal distance between the two stations (m) and f is the Coriolis parameter (e.g. Pond and Pickard, 1983). Dynamic heights are calculated directly from 2×10^4 Pa (2 dbar) files and subsampled at 2×10^5 Pa (20 dbar) intervals to retain fine scale variability.

For each station pair, if the deepest common pressure is deeper than the reference level then velocity is decreased linearly to zero in the bottom triangle, however, if the deepest common pressure is shallower than the reference level then velocities are referenced to the sea-bed and transport in the bottom triangle is zero. Reference levels are adopted

Table 1. Flow compensation components for each of the six hydrographic sections at 25° N (following Longworth, 2007). Stations refers to the number of CTD profiles made in the mid-ocean (i.e., east of the Bahamas) amounting to a section area as shown. Transports refer to annual average northward Florida Straits and Ekman transports and the southward mid-ocean transport required to maintain section mass balance (accounting for 0.8 Sv of Bering Straits inflow to the North Atlantic). The final column gives the adjustment made to geostrophic mid-ocean reference level velocities to satisfy mass balance.

			Transports (Sv)			Reference
Year	Stations	Section area ($\times 10^4$ km^2)	Florida Straits	Ekman	Mid-Ocean	Level velocity (cm s^{-1})
1957	38	2.88	31.1	4.5	−36.4	−0.13
1981	90	3.20	31.1	3.7	−35.6	−0.04
1992	101	2.96	30.3	4.6	−35.7	−0.11
1998	121	3.24	34.0	5.2	−40.0	−0.05
2004	113	3.23	31.8	4.5	−37.1	−0.01
2010	122	3.39	30.5	2.1	−33.4	−0.09

following Lavin et al. (1998) where from the eastern boundary to the start of the DWBC, an initial level of no motion is assumed at 3200 dbar. The start of the DWBC is identified from the position of an oxygen front below 1000 dbar which separates the highly oxygenated waters of the DWBC and its northward recirculation from the older, less oxygenated waters of the ocean interior (Fig. 3). In the western boundary region and to the western limit of the section, a shallower reference level of 1000 dbar is used corresponding to the transition between the northward flowing Antilles Current and the southward flowing DWBC below (e.g. Johns et al., 2008).

To satisfy mass balance in each section, a uniform section wide reference level velocity is determined to ensure southward mid-ocean transport balances northward Gulf Stream and Ekman transport with a net southward flow of 0.8 Sv remaining due to Bering Straits inflow to the North Atlantic (Table 1). Where possible (see below), annual mean Ekman transport (zonally integrated along the cruise track of each mid-ocean section) and Gulf Stream transports are obtained using the NOC v1.1 wind stress climatology (e.g. Josey et al., 2002) and cable measurements in the Florida Straits, respectively (e.g. Larsen, 1992; Meinen et al., 2010). A detailed analysis of Ekman transport and Gulf Stream transport variability at 26° N can be found in Atkinson et al. (2010).

Because the NOC v1.1 climatology covers the period 1980–2005, and Florida Straits cable transports cover the period 1982–present, Ekman transport for the 1957 and 2010 sections and Gulf Stream transport for the 1957 and 1981 sections cannot be calculated directly. For the 1957 section, Longworth (2007) used the 1980–2005 mean Ekman transport at 24.5° N, and 1982–2006 mean Gulf Stream transport, as there is little evidence for any long-term trend in either record (albeit incorporating larger error bars to account for unresolved interannual variability). An identical Gulf Stream transport is used for the 1981 section. Note that Gulf Stream transport is not obtained from the short transects made across the Florida Straits as part of the 1981–2010 sections as an undesirably large reference velocity adjustment is required such that transports match those obtained from the cable observations (referencing to the sea-bed). It is also noted that for the 1957, 1981 and 1992 sections, a mean flow of 1 Sv through the North West Providence Channel is subtracted from the Gulf Stream transport since these mid-ocean sections meet the western boundary south of this location. For the 2010 section, this study uses annual mean Ekman transports calculated from the NCEP-NCAR climatology. The switch between the NOC v1.1 and NCEP-NCAR climatology is justified because a favourable comparison is found between zonally integrated Ekman transports from the NOC v1.1 and NCEP-NCAR climatologies at these latitudes (Atkinson, 2011) though the lower spatial resolution of the NCEP-NCAR product will lead to greater uncertainty in estimating Ekman transport along the 2010 cruise track.

2.3.2 Uncertainties

The uncertainty inherent in transport estimates from one time hydrographic sections at 25° N is discussed by Longworth (2007) who highlighted a net RMS section-wide transport uncertainty of order ±6 Sv (based on work by Ganachaud, 2003) as the main limit to resolving interannual and longer term variability. This uncertainty in the assumption that each hydrographic section represents annual average conditions is dominated by the effects of eddy variability and internal waves on the baroclinic flow field. Here we use five years of continuous Rapid-WATCH transport measurements at 26.5° N to estimate this uncertainty more precisely based on observations of seasonal and sub-seasonal variability (Table 5, rightmost column).

A further source of uncertainty arises from the estimate of annual average Ekman and Florida Straits transports. This includes measurement errors and representativeness errors (e.g., the error in representing mean Florida Straits transport in 1957 using the 1982–2006 mean) and amounts to a maximum combined uncertainty of around ±2 Sv assuming errors are random (Longworth, 2007), reducing for more recent sections where annual averages are available. It is emphasised

Table 2. Mid-ocean transport error in depth classes associated with a 1 Sv error in combined Ekman and Florida Straits transport. An error in combined Ekman and Florida Straits transport leads to an error in reference level velocity and, therefore, a transport error proportional to depth class area. The transport error given is a mean error for the six hydrographic section, the final column gives the range of values about the mean for the 6 sections. Note that the AABW shows the greatest range in transport error because differing section bathymetry has the greatest effect on the area of this depth class.

Depth Class (m)	Transport Error (Sv per Sv)	Range across 6 sections (Sv)
Upper (0–800 m)	0.16	±0.01
AAIW (800–1100 m)	0.06	±0.00
UNADW (1100–3000 m)	0.37	±0.01
LNADW (3000–5000 m)	0.33	±0.01
AABW (>5000 m)	0.07	±0.02
AMOC	0.84	±0.01

that the Ekman and Florida Straits transports used in the calculations are annual mean values, so the uncertainty given for these terms is the error in estimating their annual mean transports. Hydrographic "snapshots" of mid-ocean transports are not annual mean values, so the standard deviation of Rapid-WATCH transports are used (Table 5) to estimate the uncertainty in using a "snapshot" value to represent annual mean transport in some depth layer in the presence of a noisy baroclinic flow field. For a 1 Sv error in combined Florida Straits and Ekman transport, the associated mid-ocean transport error (in depth classes) is calculated and given in Table 2. A 1 Sv change in this transport leads to an adjustment in the reference velocity required to maintain mass balance, thus, transport compensation in the mid-ocean is proportional to depth class area (and will respond linearly to changes in Florida Straits and Ekman transport error). The partitioning of Ekman and Florida Straits transport variability between mid-ocean depth levels is also a useful quantity given that Rapid-WATCH transports incorporate time variable Ekman and Florida Straits transports, but the hydrographic sections do not. This is addressed later.

Additional sources of error, such as sampling resolution and choice of reference levels, increase the uncertainty of transports observed in one time hydrographic sections. All errors should combine randomly such that the main source of uncertainty for transport in a depth layer is associated with the baroclinic flow field (typically several Sverdrups, Table 5). Combining this uncertainty with other sources of errors only tends to increase overall uncertainty by order 0.1 Sv. It is, therefore, only this baroclinic uncertainty, as estimated from Rapid-WATCH transport variability and given as standard deviations in Table 5 (right column), which is discussed in the remainder of this study, however, these further additional small sources of uncertainty should be borne in mind.

3 Results

In Sect. 3.1, changes in transport between hydrographic sections is considered in different depth classes. Definitions of the depth classes are given in Table 3 and illustrated in Fig. 4, and they follow those used in analyses of the Rapid-WATCH array (http://www.noc.soton.ac.uk/rapidmoc). Potential temperature limits for water masses of interest are also given in Table 3; it should be noted that the upper, intermediate and UNADW depth classes comprise more than one water mass within their limits. Furthermore, because the depth of the interface between water mass classes varies with time, transport variability within potential temperature classes can provide an additional useful method for decomposing transport variability and will be discussed in Sect. 3.2. The restriction of Rapid-WATCH moorings to the ocean boundaries and MAR means the conversion of the Rapid-WATCH transport-depth profiles into transport-potential temperature profiles is not trivial and will not be attempted in this study.

3.1 Transport changes in depth classes

3.1.1 Transport changes in depth layers

Transports calculated in depth classes for the six hydrographic sections are given in Table 4. The most striking result for the latest 2010 section is the partial return in strength of the total upper ocean transport (the upper limb of the AMOC) towards pre-2004 values of ≈17–18 Sv. This is due to a reduction in southward transport in the upper mid-ocean by 5.8 Sv relative to 2004, though a weak northward Ekman transport associated with a strong negative phase of the North Atlantic Oscillation (see Atkinson et al., 2010) means overall AMOC strength was still ≈1–2 Sv lower than pre-2004 levels. Even accounting for a maximum 1–2 Sv uncertainty in combined Ekman and Florida Straits northward transport used in the 2010 section (which projects on the AMOC with ≈0.8–1.6 Sv uncertainty, Sect. 2.3 and Table 2), the total upper mid-ocean transport does not approach the high southward transport of 2004. The return in strength of the AMOC towards historic values is consistent with a mean AMOC strength of 18.6 Sv from five years of Rapid-WATCH observations (2004–2009) within the large sub-seasonal and seasonal variability observed by the Rapid-WATCH array over this period (de-trended std. dev. = 4.7 Sv). The return in strength of the upper mid-ocean transport to pre-1998 values is also consistent with a mean thermocline transport of −17.6 Sv and associated std. dev. of 3.3 Sv from the Rapid-WATCH observations.

The large sub-seasonal and seasonal variability observed by Rapid-WATCH encompasses all AMOC and upper mid-ocean transport values observed in the 6 hydrographic sections within 2 standard deviations. This emphasises the difficulty of detecting lower frequency variability using snapshot hydrographic sections and prompts caution over conclusions

Table 3. Water mass definitions in depth or potential temperature (θ) classes reproduced from Longworth (2007), in turn based on the studies of Schmitz and McCartney (1993) and Fine (1995). Note that a potential temperature of 22.5 °C is chosen to separate surface and thermocline waters following investigations (Atkinson, 2011) showing this isotherm to be more representative of the base of the seasonal thermocline across the mid-ocean than the 24.5 °C isotherm used by Longworth (2007). Depth layers may contain several water mass constituents which are only identified here in temperature classes. The boundary between LNADW and AABW (1.8*) is variable and set as the shallowest occurrence of northward transport within 0.05 °C intervals (1.85 °C, 1.70 °C, 1.80 °C, 1.85 °C, 1.75 °C and 1.90 °C for the 1957, 1981, 1992, 1998, 2004 and 2010 sections, respectively). Abbreviations are: AAIW – Antarctic Intermediate Water, MW – Mediterranean Water, (S)LSW – (Shallow) Labrador Sea Water, NAIW – North Atlantic Interior Water, ISOW – Iceland Scotland Overflow Water, DSOW – Denmark Straits Overflow Water, AABW - Antarctic Bottom Water.

Layer	Depth Limits (m)	Constituents	θ Limits (°C)
Upper	$z \leq 800$	Surface	>22.5
		Thermocline	$12.5 < \theta \leq 22.5$
		Lower Thermocline	$9.5 < \theta \leq 12.5$
Intermediate	$800 < z \leq 1100$	AAIW and MW	$5 < \theta \leq 9.5$
UNADW	$1100 < z \leq 3000$	SLSW	$4 < \theta \leq 5$
		LSW	$3.2 < \theta \leq 4$
		NAIW and ISOW	$2.5 < \theta \leq 3.2$
LNADW	$3000 < z \leq 5000$	DSOW	$1.8^* < \theta \leq 2.5$
AABW	$z > 5000$	AABW	$\theta \leq 1.8^*$

that enhanced upper-ocean gyre circulation in the 1998 and 2004 sections is indicative of a new, weaker AMOC state (Bryden et al., 2005b). Note also that in this study the AMOC strength was not low in 1998 (Table 4) due to enhanced northwards Florida Straits and Ekman transports, demonstrating the importance of accounting for interannual variability in these components where mid-ocean transport is considered representative of the annual mean. In the deep ocean, a return in strength of the lower AMOC limb towards historic levels in 2010 (relative to 2004) is achieved mostly by a 4.3 Sv enhancement of southward transport of UNADW. Southward transport of LNADW weakened by 2.1 Sv in 2010 relative to 2004, maintaining the apparent weakened state observed in the 1998 and 2004 sections. Bryden et al. (2005b) argued that this weakening of the LNADW in the 1998 and 2004 sections was evidence that the lower limb of the AMOC itself had weakened because of the distinct vertical structure of the changes. Whilst the enhancement of the AMOC back towards historic strength in 2010, despite weakened LNADW transport, demonstrates this is not necessarily true, the continued weakened LNADW strength and record UNADW strength in the 2010 section forms a curious new vertical transport structure that warrants further investigation. It is noted that both the UNADW and LNADW 2010 transports are consistent with the 5-year means and std. dev. from the

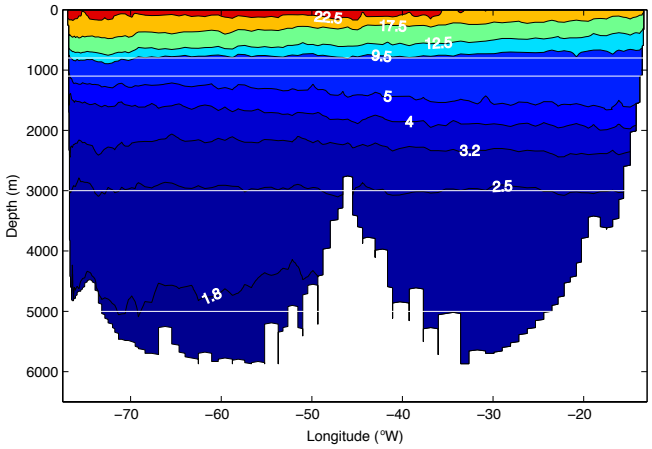

Fig. 4. Potential temperature at 25° N for the 2004 hydrographic section; contours correspond to the class partitions given in Table 3 (note that the 17.5 °C isotherm is also plotted). Depth levels of 800 m, 1100 m, 3000 m and 5000 m are shown.

Rapid-WATCH observations; these are -12.2 ± 2.8 Sv and -8.1 ± 2.7 Sv, respectively. Both the AABW and Intermediate water transports show no major changes in the 2010 section and are also consistent with Rapid-WATCH observations of 2.1 ± 0.5 Sv and 0.5 ± 0.6 Sv, respectively.

3.1.2 Mid-ocean transport profile variability

To further investigate the vertical structure of the changes, profiles of transport per unit depth for the hydrographic sections are compared to similar profiles from the Rapid-WATCH observations. At each time step, Rapid-WATCH observations of geostrophic mid-ocean transport have a hypsometric (near barotropic) transport adjustment applied to maintain mass balance through the section (Kanzow et al., 2010, transport imbalance is divided by section area to obtain a compensation velocity which is then applied uniformly across the section). Because Rapid-WATCH observations incorporate time variable Ekman and Florida Straits transport observations (which project on mid-ocean transports as per Table 2), to compare these with the hydrographic data it is necessary to re-compute Rapid-WATCH mid-ocean transports using time-mean Ekman and Florida Straits transports. In both the Rapid-WATCH data and on longer timescales, the greatest Ekman and Florida Straits transport variability occurs at seasonal and sub-seasonal timescales (Kanzow et al., 2010; Atkinson et al., 2010) where mid-ocean compensation is expected to be barotropic (Jayne and Marotzke, 2001; Kanzow et al., 2007; Bryden et al., 2009), thus, a depth independent mode of variability is expected to be removed. Accordingly, variability in the upper ocean, UNADW and LNADW is reduced from std. devs. of 3.3, 2.8 and 2.7 Sv to std. devs. of 3.1, 2.3 and 2.3 Sv, respectively, once Ekman and Florida Straits variability is removed. The resulting Rapid-WATCH profiles only show mid-ocean transport variability associated

Table 4. Northward transport (Sv) in depth classes for the six hydrographic sections. The upper layer comprises transport in the Ekman layer, Florida Straits and mid-ocean (≤800 m), the lower layer comprises mid-ocean only (>800 m); for full class definitions see Table 3. Ekman transports (zonally integrated across 25° N) and Florida Straits transports are annual averages calculated from wind stress climatologies and cable observations, respectively (Sect. 2.3). Net imbalance between upper and lower layer total transports is due to Bering Straits inflow (0.8 Sv) to the North Atlantic.

		1957	1981	1992	1998	2004	2010
Upper	Ekman	4.5	3.7	4.6	5.2	4.5	2.1
	Florida Straits	31.1	31.1	30.3	34.0	31.8	30.5
	Mid-Ocean	−15.9	−18.0	−17.2	−22.2	−23.4	−17.2
	Total	19.7	16.8	17.7	17.0	12.9	15.4
Lower	Intermediate	1.6	1.1	0.7	−0.3	0.8	0.7
	UNADW	−11.8	−9.3	−11.1	−12.9	−10.4	−14.7
	LNADW	−12.6	−12.2	−10.5	−5.8	−6.6	−4.5
	AABW	2.3	2.9	2.4	1.1	2.5	2.3
	Total	−20.5	−17.5	−18.5	−17.9	−13.7	−16.2

with changes in mid-ocean vertical transport structure. Finally, variability at each depth is low-passed at 10-day period (vertical profile data is initially made available low-passed at two-day period) which is the shortest period at which Rapid-WATCH resolves AMOC variability (Kanzow et al., 2007).

To eliminate any mid-ocean transport variability associated with inter-annual Ekman and Florida Straits transport variability in the hydrographic sections (where mass balance is maintained through the application of a section-wide compensation velocity, see Tables 1 and 2), mid-ocean transports are recalculated using long-term mean Ekman and Florida Straits transports. These are given in Table 5. The long-term mean Ekman transport used is the 1980–2005 mean transport calculated using the NOC v1.1 climatology and the long-term mean Florida Straits transport used is the 1980–2007 mean calculated from cable observations. Note that Florida Straits transport is reduced by 1 Sv in the 1957, 1981 and 1992 sections to account for flow through the North West Providence Channel. When comparing hydrographic transports with those from Rapid-WATCH, a zero net section-wide transport constraint is also used during the calculation of hydrographic transports (i.e., an inflow of 0.8 Sv into the North Atlantic through the Bering Strait is ignored) consistent with the mass balance approach used by Rapid-WATCH.

The resulting geostrophic vertical transport per unit depth profiles for the hydrographic and Rapid-WATCH data are shown in Fig. 5. These incorporate a mean transport per unit depth profile for the Florida Straits in the upper 800 m but exclude mean surface Ekman transport. To obtain a vertical transport profile from mean total cable transport, coefficients identical to those of Longworth (2007) were used which represent a linear regression of Florida Current transport in 10 m bins against total transport. This regression analysis makes use of 65 PEGASUS sections completed in 1982–1984 during which free-falling instruments were used to measure absolute velocity and temperature (Leaman et al., 1987; Shoosmith et al., 2005). Multiplying these coefficients by mean Florida Straits transport gives a mean transport per unit depth profile. Figure 6 shows upper ocean transport per unit depth profiles for the full section (including mean Florida Straits transport per unit depth) and just the mid-ocean. It is reiterated that these profiles show just variability associated with the mid-ocean and, thus, indicate how the mid-ocean hydrographic transport profile structures compare with the mid-ocean sub-seasonal and seasonal variability observed by Rapid-WATCH.

It is immediately obvious from Figs. 5 and 6 that the mid-ocean hydrographic transport profile variability falls within the range of Rapid-WATCH variability in the upper 4800 m of the water column, and the shape of the profiles is comparable to those observed by Rapid-WATCH. The pronounced strengthening of southward UNADW transport and weak southward LNADW transport in the 2010 section falls within the range of "s" shaped profiles observed by Rapid-WATCH between 1000–5000 m, suggesting this state is not unusual. The same is true of the 1998 and 2004 sections whose weak southward LNADW transports (relative to earlier hydrographic sections) also fall in the envelope of Rapid-WATCH transport profiles. This is emphasised in Table 5 where UNADW and LNADW mid-ocean variability for all 6 hydrographic sections falls within ±2 std. dev. of the mean Rapid-WATCH transports. In the upper mid-ocean, stronger southward transports in the 1998 and 2004 sections also fall within the envelope of Rapid-WATCH transport profiles. Interestingly, the particularly strong southward transport observed in the 2004 hydrographic section (Table 5) has a vertical transport profile that reaches the limit of the Rapid-WATCH envelope between 100–200 m (Fig. 6). Whilst this state lies at the edge of this envelope, its vertical structure is not unique and appears comparable to a small number of Rapid-WATCH

Table 5. Northward transport (Sv) in depth classes for the six hydrographic sections calculated using long-term mean Ekman and Florida Straits transports (thus, isolating interior ocean variability). Numbers in italic denote transports adjusted for seasonal variability derived from 5 years of Rapid-WATCH observations (2004–2009). Rapid-WATCH transports are also calculated using long-term mean Ekman and Florida Straits transports. For each depth class, Rapid-WATCH timeseries transport properties are given (right-most column), these are: mean transport/seasonal cycle range (upper), std. dev./std. dev. with seasonal cycle removed (lower). Depth class definitions are from Table 3.

	1957	1981	1992	1998	2004	2010	Rapid
Ekman	4.5	4.5	4.5	4.5	4.5	4.5	3.6
Florida Straits	31.1	31.1	31.1	32.1	32.1	32.1	32.1
Mid-Ocean	−15.7	−18.0	−17.2	−21.6	−23.3	−17.7	−17.6/7.6
(0–800 m)	*−19.0*	*−18.9*	*−17.4*	*−19.8*	*−21.4*	*−16.9*	3.1/2.4
Upper total	19.9	17.6	18.4	15.0	13.3	18.9	18.1/7.6
	16.6	*16.7*	*18.2*	*16.8*	*15.2*	*19.7*	3.1/2.4
Intermediate	1.6	1.1	0.7	−0.0	0.8	0.5	0.5/1.0
(800–1100 m)	*1.4*	*0.9*	*0.4*	*0.0*	*0.9*	*0.6*	0.6/0.5
UNADW	−11.5	−9.3	−11.0	−11.6	−10.2	−15.9	−12.3/5.9
(1100–3000 m)	*−8.9*	*−8.4*	*−11.0*	*−13.4*	*−10.8*	*−17.1*	2.3/1.8
LNADW	−12.3	−12.3	−10.4	−4.6	−6.5	−5.6	−8.2/2.6
(3000–5000 m)	*−11.5*	*−12.0*	*−10.0*	*−4.9*	*−7.5*	*−5.3*	2.3/2.2
AABW	2.3	2.8	2.4	1.4	2.5	2.0	2.0/0.5
(>5000 m)	*2.4*	*2.8*	*2.4*	*1.4*	*2.3*	*2.2*	0.5/0.4
Lower total	−19.9	−17.6	−18.4	−15.0	−13.3	−18.9	18.1/7.6
	−16.6	*−16.7*	*−18.2*	*−16.8*	*−15.2*	*−19.7*	3.1/2.4
Cruise Month	Oct	Aug–Sep	Jul–Aug	Feb	Apr	Jan–Feb	–

transport profiles that also show a similar kinked structure in the near-surface ocean. Also interesting is the return in strength of the 2010 upper mid-ocean transport to pre-1998 values, which in part appears due to a pronounced weakening of southward transport within a few hundred metres of the surface. This is typical of the mean transport profile as measured by Rapid-WATCH (Fig. 5), suggesting some enhanced southward transport may persist in the main thermocline. This will be revisited in Sect. 3.2.

Below 4800 m, Rapid-WATCH interpolates mooring profiles onto a historical mean AABW profile estimated from the pre-2010 hydrographic sections (Kanzow et al., 2010), thus, it does not fully resolve variability at these depths. No effort is, therefore, made to compare hydrographic with Rapid-WATCH data in this depth range. Frajka-Williams et al. (2011) show that six months of AABW transport from mooring observations have a range of transport from 1–3 Sv with a standard deviation of 0.4 Sv and conclude that short-term variability in AABW transport complicates the inference of longer term changes in the hydrographic sections.

Figures 5 and 6 and the associated transports in depth classes given in Table 5 emphasise that changes in mid-ocean transport observed by the hydrographic sections are not significant in terms of the sub-seasonal and seasonal variability observed by Rapid-WATCH.

3.1.3 Seasonal cycles from five years of Rapid-WATCH data

Although the mid-ocean hydrographic changes do not appear significant in terms of the variability observed by Rapid-WATCH, one possible reason may be the aliasing of any mid-ocean seasonal cycles. Kanzow et al. (2010) used four years of Rapid-WATCH data to identify a strong seasonal cycle in the AMOC at 26.5° N with peak to trough amplitude of 6.7 Sv. The chief contributor to this seasonal cycle is geostrophic mid-ocean variability which is largely attributable to wind stress curl forcing at the eastern boundary of the Atlantic. This suggests that aliasing of the seasonal cycle in the hydrographic sections could play a significant role in the observed changes. To investigate this, mid-ocean seasonal cycles are calculated (i.e., still using long-term mean Florida Straits and Ekman transport) for the depth classes in Table 3. These are plotted as timeseries in Fig. 7 and with five years of data overlaid in Fig. 8 (left column, red lines) and are estimated by applying a 60-day low-pass filter to the means of each twice daily Rapid-WATCH observation (i.e., the mean of all 1 January's, 2 January's, etc.). Seasonal anomalies are then subtracted from the hydrographic values using the mean anomaly for the months over which each cruise took place. Seasonally adjusted transports are shown

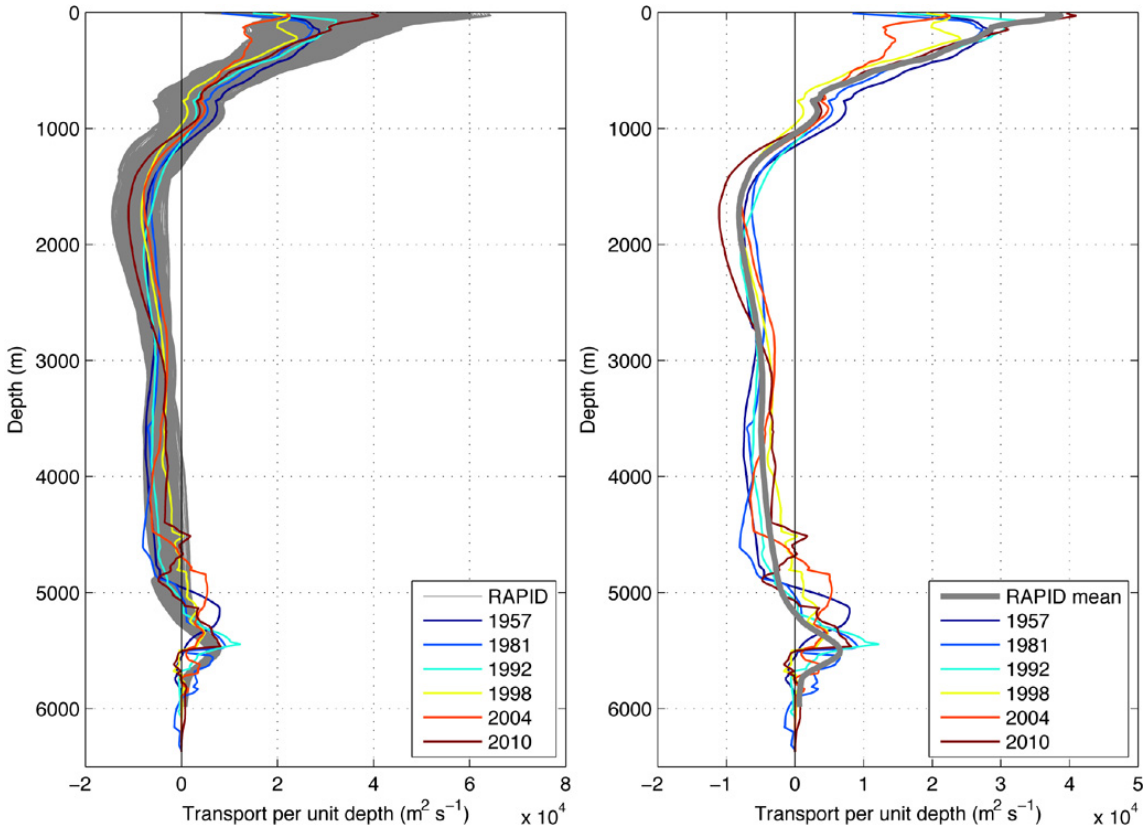

Fig. 5. Profiles of total transport per unit depth (excluding mean surface Ekman transport) for the 6 hydrographic sections and 5 years of Rapid-WATCH data (April 2004–April 2009). Rapid-WATCH data are shown in grey, the grey envelope in the left plot comprises 3562 Rapid-WATCH profiles (available twice daily for 5 years) whilst the grey line in the right plot shows the mean of these profiles. All profiles use long-term mean Florida Straits and Ekman transport, thus, variability represents only that associated with changes in mid-ocean vertical transport structure.

in italics in Table 5, along with seasonal cycle range for each depth class and the dates of each cruise.

In the upper ocean, the seasonal cycle is reasonably well defined relative to the 5-year spread of the data (Fig. 8) with a southward maximum in Spring, a minimum in Autumn, and a secondary maximum in mid-Winter, in agreement with Kanzow et al. (2010). However, the 7.6 Sv range of the upper mid-ocean seasonal cycle (Table 5) is 1.7 Sv larger than the 5.9 Sv range calculated by Kanzow et al. (2010) using 4 years of Rapid-WATCH data (2004–2008). The majority of the increase comes from the use of a 60-day low-pass filter on the 5-year daily averages to estimate the seasonal cycle, which has a seasonal range that is 1.5 Sv greater than for simple monthly averages. This occurs because the seasonal maximum, and particularly minimum southward transports, fall on boundaries between adjacent months. The filtering approach used in this study is thus considered a better approach for estimating the seasonal cycle in the Rapid-WATCH data.

In the deep ocean, the UNADW seasonal cycle is also reasonably well defined relative to the 5-year spread of the data (Fig. 8) with a southward transport minimum in Spring, a maximum in Autumn and a range of 5.9 Sv (Table 5). In the LNADW a somewhat similar structure still exists with a southward transport minimum in Spring and a maximum in Winter, but with a much smaller range of 2.2 Sv and a less well defined cycle relative to the 5-year spread of the data (Fig. 8). Broadly though, the data suggest a first mode like internal variability of the mid-ocean flow, consistent with the conclusions of Kanzow et al. (2010) who identified wind stress curl forced Ekman pumping at the eastern boundary as the chief mechanism driving this variability. At intermediate water depths (800–1100 m), the seasonal cycle shows some coherence with the upper ocean, consistent with Chidichimo et al. (2010) who found that seasonal upper ocean density anomalies close to the African coastline are coherent to depths of ≈1400 m (in the first 3.5 years of Rapid-WATCH data) and that most transport variability there has a first-mode type structure.

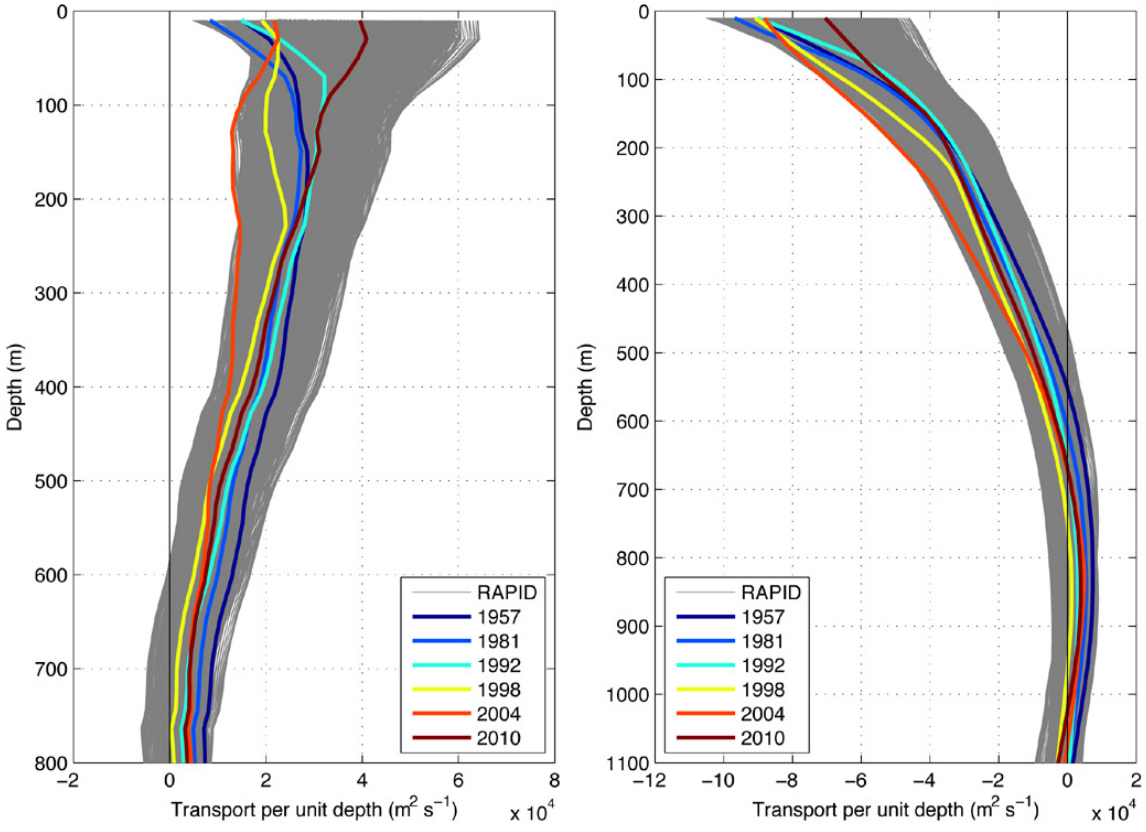

Fig. 6. Transport per unit depth profiles as for Fig. 5, but showing only the upper ocean. The left plot shows total upper ocean transport (excluding mean surface Ekman transport), the right plot shows mid-ocean transport (excluding mean surface Ekman transport and mean Florida Straits transport per unit depth).

3.1.4 Mid-ocean hydrographic transport variability with seasonal effects removed

Adjusting the upper-ocean hydrographic data to take account of this seasonal anomaly, the enhanced southward transport in 1998 and 2004 is less well defined, suggesting that part of the weakening AMOC trend identified by Bryden et al. (2005b) using the pre-2010 data was the result of aliasing enhanced southward transport in the mid-ocean seasonal cycle during late Winter and early Spring (Fig. 8). The remaining upper ocean hydrographic variability lies comfortably within two std. dev. of the mean Rapid-WATCH transport of −17.6 Sv (the std. dev. for the de-trended and de-seasonalised 5 year timeseries is 2.4 Sv, see Table 5), i.e., within the range of sub-seasonal variability. No significant long-term transport variability can, therefore, be identified from the de-seasonalised upper ocean hydrographic transports. Kanzow et al. (2010) also de-seasonalised the work of Bryden et al. (2005b) to obtain a similar result in the upper-ocean, though they did not isolate mid-ocean variability nor did they compare identical depth ranges.

In the deep ocean, the greater amplitude of the seasonal cycle in the UNADW relative to the LNADW leads to a larger seasonal adjustment to hydrographic transports in this depth class (Fig. 8). In the LNADW, the removal of a small seasonal bias does not affect the long-term weakening trend, whilst in the UNADW removal of a seasonal bias emphasises a long-term strengthening trend (particularly through adjustment of the 1957 and 1981 UNADW transports towards a weaker southward flow, Fig. 8). Whilst the 5-year Rapid-WATCH UNADW and LNADW timeseries show similar std. dev., the greater amplitude of the UNADW seasonal cycle relative to the LNADW means the std. dev. of sub-seasonal variability in the UNADW is smaller than for the LNADW (Table 5). In the UNADW, the seasonally adjusted hydrographic values for 1981 and 2010 are found to lie outside ±2 std. dev. (for the de-trended and de-seasonalised timeseries) of the Rapid-WATCH mean (-12.3 ± 3.6 Sv) suggesting some longer term change is very likely to have taken place outside the range of sub-annual variability. In the LNADW, no seasonally adjusted values lie outside ±2 std. dev. of the Rapid-WATCH mean (-8.2 ± 4.4 Sv) though the 1981 value lies within 0.6 Sv of the lower limit. The fact that some significant (and near significant) interannual or longer term changes do appear to have occurred warrants further investigation and will be addressed in Sect. 3.2. Changes in

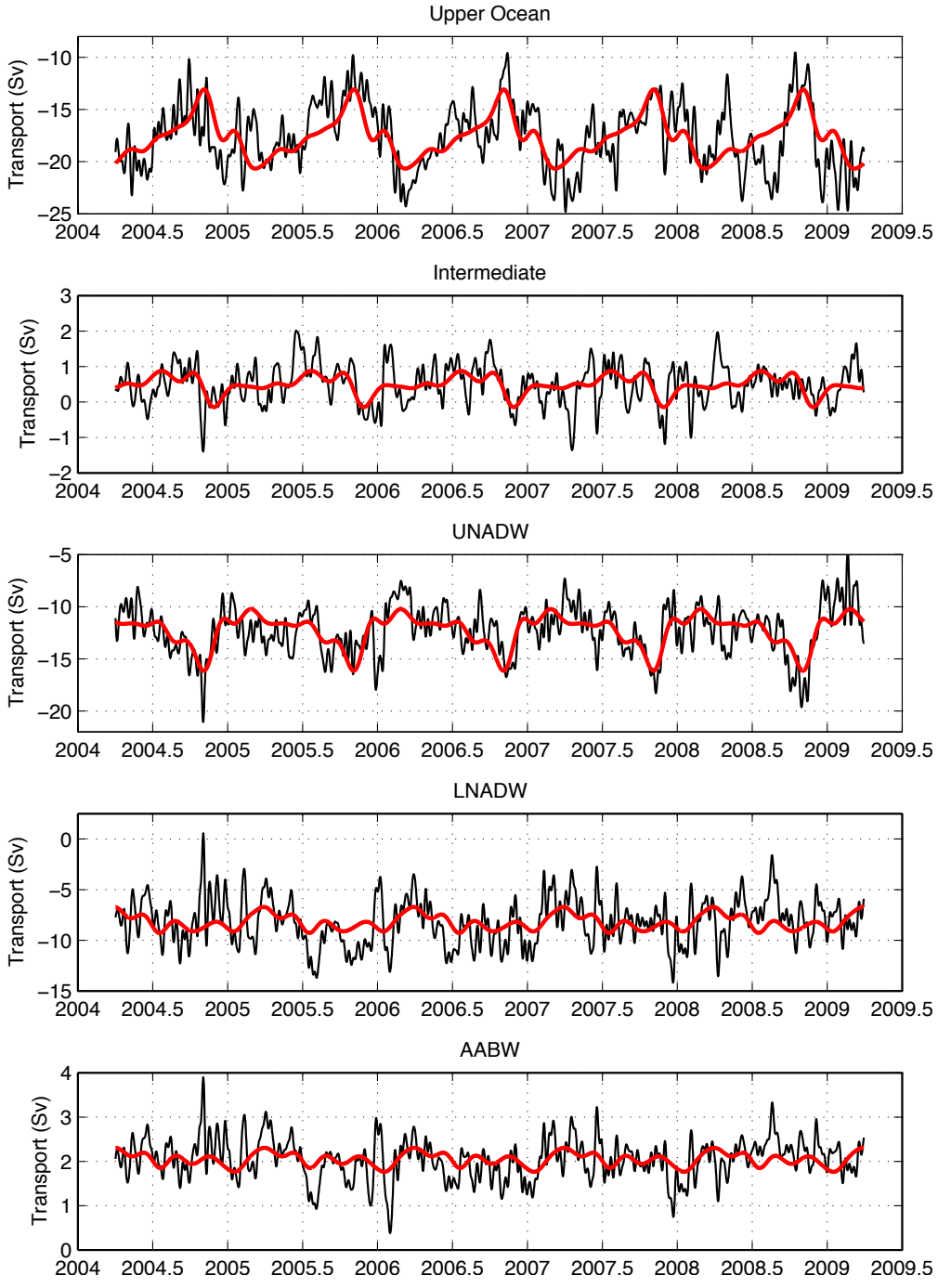

Fig. 7. April 2004–April 2009 Rapid-WATCH transport timeseries at 26.5° N (black) with the mean seasonal cycle overlaid (red). Mid-ocean timeseries are calculated using time-mean Ekman and Florida Straits transports (to isolate mid-ocean variability). Seasonal cycles are calculated from the 5-year mean of each twice daily value (i.e., all 1 January's, all 2 January's, etc.) which are then 60-day low-pass filtered to obtain the seasonal cycle.

the intermediate water are not significant relative to Rapid-WATCH data whilst AABW and Rapid-WATCH data are not readily comparable (as stated earlier) and are included here only for completeness.

In making seasonal adjustments to the hydrographic data, it is assumed that the seasonal cycles calculated at 26.5° N using the 5-year Rapid-WATCH dataset are persistent over the time and space scales of the hydrographic observations. Based on an analysis of wind stress at the African margin,

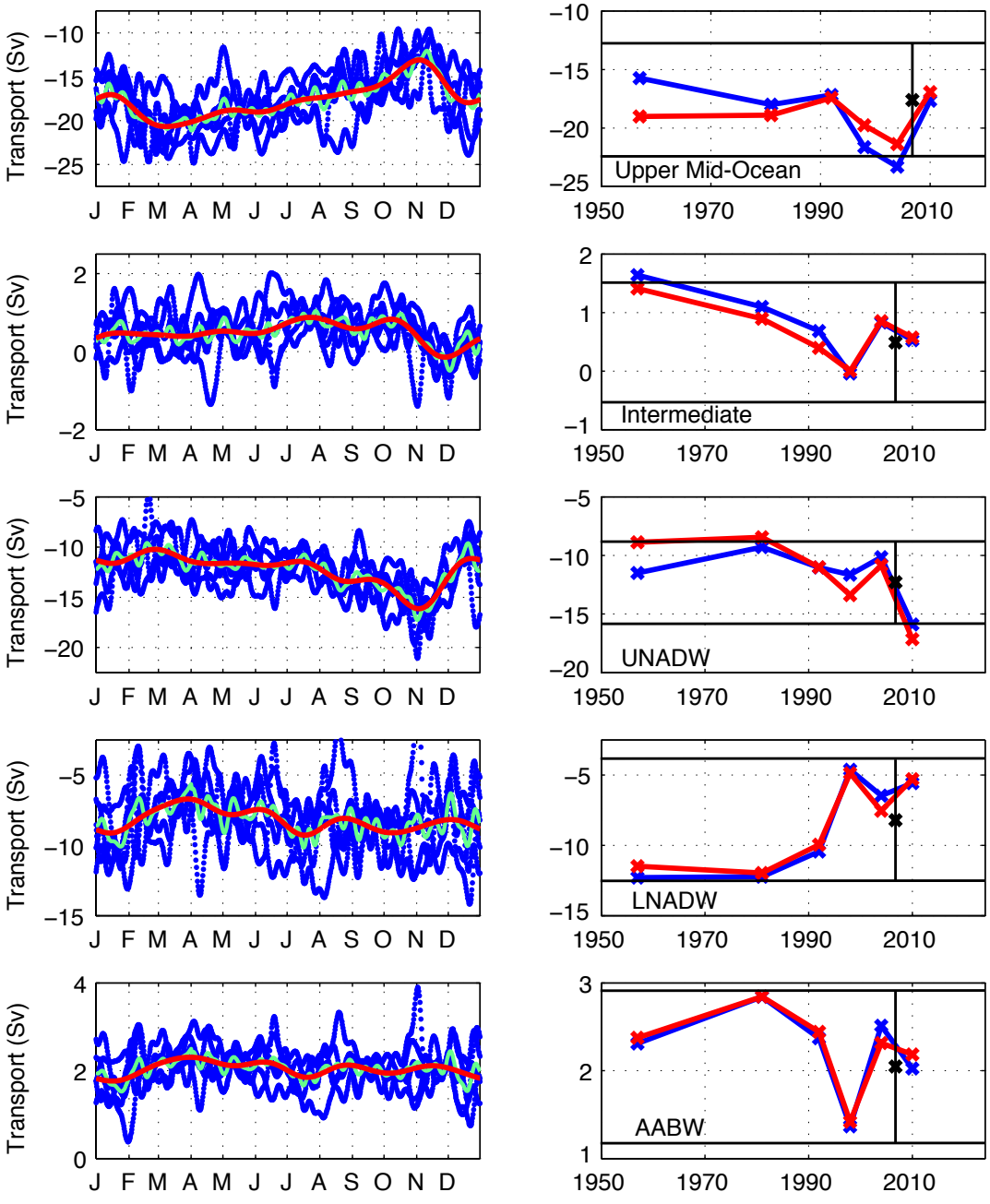

Fig. 8. Left column, seasonal transport cycles (red lines, as for Fig. 7) calculated in depth classes given in Table 3 for five years of Rapid-WATCH data (2004–2009). Blue lines denote each year of data overlaid (10-day low-pass filtered), fine green lines show the 5-year mean of each twice daily value (i.e., all 1 January's, all 2 January's etc.) which are then 60-day low-pass filtered to obtain the seasonal cycle (red lines). Right column, lines denote mid-ocean transport for the 6 hydrographic sections with (red) and without (blue) adjustment for seasonal anomalies (see also Table 5). Black bars denote the mean of the Rapid-WATCH data ±2 std. dev. of the de-trended and de-seasonalised 5-year timeseries. In addition to the ±2 std. dev. shown, hydrographic transport estimates will have a further uncertainty of order 0.1 Sv associated with other sources of error (Sect. 2.3).

Kanzow et al. (2010) suggest that AMOC seasonal anomalies seen in the Rapid-WATCH data are likely to be observed over space and time scales exceeding that of the Rapid-WATCH observations, which supports removal of a seasonal transport anomaly from the six hydrographic sections. The removal of a seasonal transport anomaly is more robust for the 1981, 1998, 2004 and 2010 sections whose cruise tracks closely follow the Rapid-WATCH mooring positions. For the 1957 and 1992 sections, removal of Rapid-WATCH seasonal transport anomalies is less certain due to a more southerly cruise

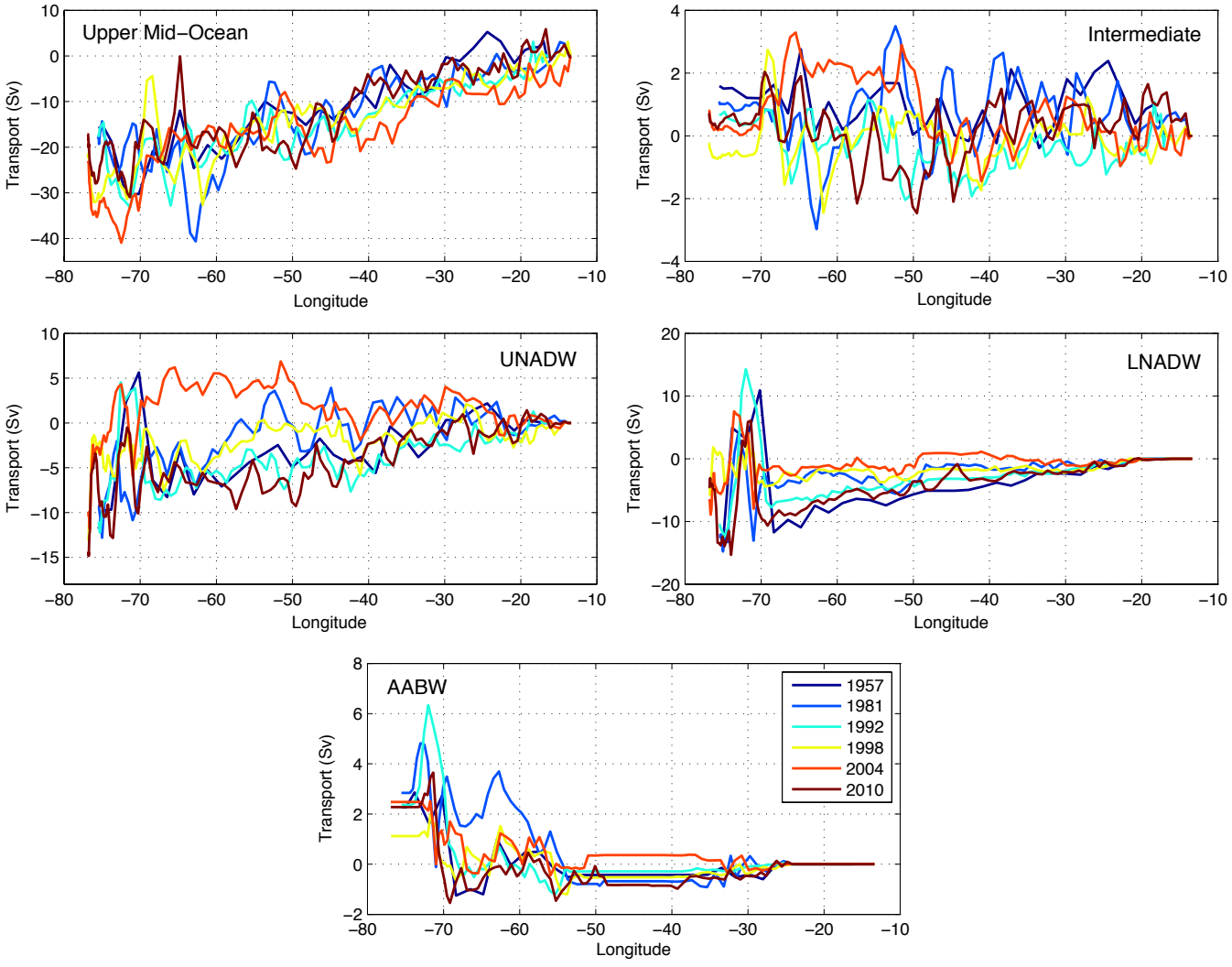

Fig. 9. Cumulative mid-ocean transport summed from east to west for the 1957, 1981, 1992, 1998, 2004 and 2010 hydrographic sections (following Longworth, 2007). Depth intervals are given in Table 3.

track approaching the African margin (Fig. 1). For the above results, it is the earlier 1981 and 1957 UNADW and LNADW transports that show the most interesting differences relative to Rapid-WATCH measurements. It is emphasised, however, that the differences in 1957 and 1981 LNADW transports relative to Rapid-WATCH are not reliant on the removal of a seasonal transport anomaly to become apparent.

3.1.5 The zonal structure of transport changes

The longitudinal structure of transport changes between the six hydrographic sections is presented in Fig. 9 using east to west cumulative transport profiles for the depth layers in Table 3. The transports used are those given in Table 4, i.e., using annual average Ekman and Florida Straits transports, though the structures of mid-ocean changes are robust whether or not these annual means are used and does not change the investigation of mid-ocean transport variability as presented in Fig. 9.

In the upper ocean, some evidence is seen of the seasonal transport variability described above. Chidichimo et al. (2010) compared two density profiles, one from merged mooring data up the eastern margin, and one from a full depth mooring located at 24° W (EB1, see Fig. 2) and found little coherence, demonstrating that most of the AMOC seasonal cycle observed by Rapid-WATCH is confined locally to the eastern margin and coherent over the upper 1400 m of the water column. In a cumulative transport plot beginning at the eastern margin, it is expected that both the 1998 and 2004 (Winter–Spring) sections would accumulate enhanced southward transport east of 24° W relative to the 1957 and 1981 sections (Summer–Autumn) of order several Sverdrups due to an opposing phase of seasonal cycle. This is observed for the 2004 section which shows enhanced

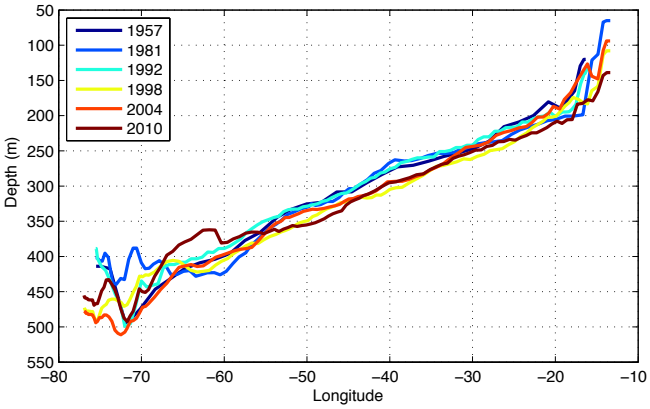

Fig. 10. Depth of the 17 °C isotherm across the mid-ocean for the 1957, 1981, 1992, 1998, 2004 and 2010 hydrographic sections (following Longworth, 2007). Values are smoothed using a ±4° longitude running mean between 70° W and 20° W and a ±1° window west and east of this at the ocean margins.

cumulative southward transport over most of this longitudinal range before merging with the other sections at ≈25° W, but a distinct ordering amongst cumulative transports dependent on predicted seasonal phase is not obvious. Evidence of seasonal Ekman pumping at the eastern margin is further investigated in Fig. 10 using the depth of the 17 °C isotherm. For the 1981, 1998, 2004 and 2010 sections, which deviate northwards approaching Africa, evidence of enhanced Winter/Spring Ekman pumping is observed between 25° W–16° W where for the 1998 and 2004 sections the isotherms are displaced toward the surface of order tens of metres relative to 1981. East of ≈16° W, the 17 °C isotherm rises steeply toward the surface which is due to a coastal upwelling regime. For the July 1981 section, the 17 °C isotherm rises by ≈140 m close to the African coast which almost coincides with a Summer maximum in southward coast-parallel trade winds, though the effect of this is not evident in the cumulative transport plots. The 1957 and 1992 sections do not show a relative seasonal deepening of the 17 °C isotherm, though these sections were occupied several degrees south of the Rapid-WATCH array at these longitudes. Overall it is hard to find strong evidence of the seasonal cycle observed by Rapid-WATCH in the hydrographic sections.

Across the remainder of the upper ocean a general southward flow is observed, locally disrupted by eddy activity (Fig. 9). East of ≈70° W, all cumulative profiles tend to intertwine before noisily separating towards their final zonally integrated values closer to the western margin. This behaviour is indicative of enhanced eddy activity at the western margin. The horizontal structure of the hydrographic transport variability in the upper ocean is consistent with the earlier result that all upper ocean transport variability falls within the range of sub-seasonal variability observed by Rapid-WATCH. Enhanced eddy activity approaching the western margin is also seen for the five year Rapid-WATCH dataset, where the western margin is found to make a greater contribution to zonally integrated upper ocean transport variability than the eastern margin (2.8 Sv RMS and 2.3 Sv RMS, respectively, after Gulf Stream and Ekman transport variability is removed) despite possessing a weaker seasonal cycle than the eastern margin (Kanzow et al., 2010). Although eddy activity has been shown to diminish sharply approaching the western margin at these latitudes, its effect on basinwide integrated volume transports is still substantial, contributing ≈2.3 Sv RMS to zonally integrated transport variability in the upper ocean (Kanzow et al., 2010).

In the UNADW, cumulative transports shows no clear evidence of differing seasonal phase east of ≈25° W where, as for the upper ocean, much of the seasonal mid-ocean transport cycle is expected to occur (Fig. 9). Further west a mostly southward mid-ocean transport accumulates across the basin width, except for the 2004 section where northward transport above the mid-ocean ridge leads to a net northward transport in the ocean interior. West of ≈70° W, the mean structure of the UNADW transports differs somewhat for the earlier three sections whose cruise tracks do not deviate north towards the Florida Straits (Fig. 1). In the 1957, 1981 and 1992 sections, a broader western boundary current with strong offshore recirculation gyre (not evident in the 1981 section) seems to be observed whilst in the 1998, 2004 and 2010 sections a narrower and stronger western boundary current adjacent to the basin margin is seen. Similar to the upper ocean, cumulative profiles tend to separate noisily towards their final zonally integrated values approaching the western margin, indicative of enhanced eddy variability in this region and consistent with the earlier observation that most hydrographic variability falls close to the range of sub-seasonal variability observed by Rapid-WATCH. The structure of any interannual or longer term transport changes in DWBC transport that may be occurring in this region is difficult to separate from shorter term variability.

In the LNADW, for all six sections southward transport accumulates gradually across the basin width and eddy activity is somewhat diminished in comparison with shallower depths. West of ≈68–70° W, all sections show evidence of a southward flow approaching the basin margin which is inshore of a broader offshore recirculation gyre. This appears less well developed for the 1998 and 2004 sections resulting in a weaker southward transport at the margin. The 2010 section shows a particularly interesting structure in this region where despite having a significantly stronger southward transport across the mid-ocean in comparison with the 1998 and 2004 sections, a strong northward transport occurs close to the western margin to give a final, comparatively weak section wide transport. As for the UNADW, it is difficult to identify any coherent structure in the changes in LNADW transport such that longer term changes could be separated from shorter term variability. This seems consistent with all

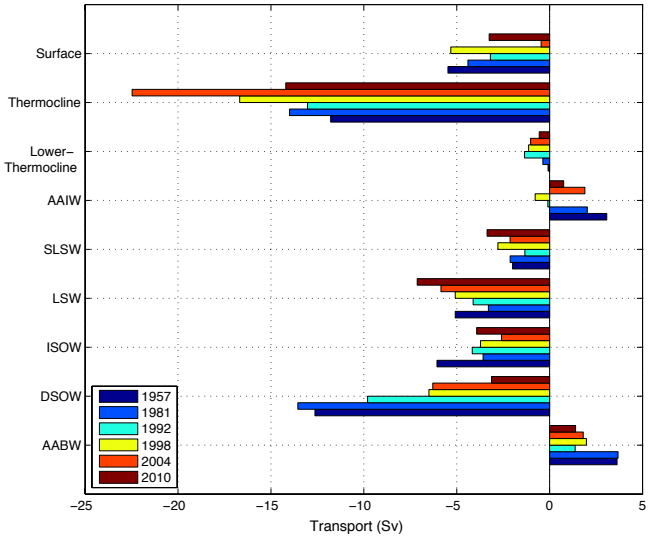

Fig. 11. Mid-Ocean transport for the six hydrographic sections in the potential temperature classes given in Table 3.

LNADW hydrographic transport variability also falling close to the range of Rapid-WATCH sub-seasonal variability.

Consistent with the hydrographic data (Fig. 9), for the five year Rapid-WATCH dataset, in the deep ocean the western margin makes a greater contribution to zonally integrated transport variability than the eastern margin (1.7 versus 1.6 Sv RMS for the UNADW and 2.1 versus 1.4 Sv RMS for the LNADW). Overall, for the hydrographic data, large-scale and longer period zonally integrated transport changes are difficult to separate from localised eddy variability in the western boundary region which is of comparable or greater magnitude.

3.2 Transport changes in potential temperature classes

3.2.1 A comparison with changes in depth classes

Because the depth of the interface between water masses of interest varies with time, it is useful to also consider water mass changes in potential temperature classes (Table 3) for the six hydrographic sections (Table 6). Most of the mid-ocean changes in potential temperature classes are broadly consistent with those seen in Table 4 over their typical depth range, which is due to the near horizontal nature of isotherms at 25° N (Fig. 4) and because most transport changes in potential temperature classes occur primarily due to changes in the velocity field and not the thickness of the layers of interest (the full decomposition of transport changes in potential temperature classes into contributions from velocity changes and changes in cross-sectional area can be seen in Atkinson, 2011). In the upper ocean, total transport variability between the hydrographic sections in potential temperature classes is similar to that in depth classes, but with total transports that are generally 2–3 Sv lower. This is due to mid-ocean northward Antarctic Intermediate Water transport being separated from upper ocean transport, and deep northward Florida Straits transport (<9.5 °C) being classified as intermediate water. Total southward transports in the lower ocean are similarly affected and are 2–3 Sv higher than those in depth classes. The use of potential temperature classes allows variability to be sub-divided more finely into source regions of particular interest, such as main thermocline water, Labrador Sea water and Denmark Straits overflow water, and reveals some interesting changes not observed in depth classes. These are considered below.

3.2.2 Transport changes in potential temperature layers

The transport changes given in Table 6 for potential temperature classes are visualised in Fig. 11 for the mid-ocean. Southward thermocline transport in the 1998, and particularly 2004 sections is enhanced relative to the 2010 and earlier sections, consistent with the transport profiles seen in Fig. 6. The strong southward thermocline transport seen in the 2004 section is in part due to cold surface temperatures and the partitioning of southward surface geostrophic transport into the thermocline. However, if an isotherm of 22.0 °C is used to separate surface and thermocline waters, a southward transport of 20.1 Sv is still observed, suggesting enhanced thermocline transport in the 2004 section (by ≈7–9 Sv relative to the 1957, 1981 and 1992 sections) is a robust result. If transport changes are considered in finer potential temperature divisions (not shown), most of the enhanced southward transport in the 2004 section occurs in the warmer 18.5–22.5 °C thermocline waters.

The 1998, 2004 and 2010 thermocline waters may have an enhanced southward transport associated with a strong seasonal transport cycle of >7 Sv range which occurs close to the eastern margin in the upper ocean at these latitudes (Fig. 7). Whilst it is not yet possible to partition this seasonal transport cycle into potential temperature classes, it is likely that this will have a similar effect on the thermocline waters. As enhanced southward thermocline transport in the 1998 and particularly 2004 sections is within the seasonal cycle range at 26.5° N (and given sub-seasonal eddy variability of order 2–3 Sv RMS, Table 5), this cannot be confidently attributed to any potential longer term increase in southward gyre transport. Interestingly, in the mid-ocean the 17.5 °C isotherm is depressed across much of the mid-ocean in the 1998, 2004 and 2010 sections relative to the 1957, 1981 and 1992 sections (Fig. 10), and the thickness of the thermocline is enhanced section-wide by ≈20 m in the 1998 and 2004 sections relative to the mean for all sections. Although seasonal and sub-seasonal transport variability may obscure evidence of longer term transport variability in the upper ocean, Ekman pumping and southward gyre transport may have increased over time, as suggested by some wind stress climatologies at 26° N (Atkinson et al., 2010).

Table 6. Northward transport (Sv) in potential temperature classes for the six hydrographic sections; for full class definitions see Table 3. Layer totals are also given. Note that net imbalance between upper and lower layer total transports is due to Bering Straits inflow (0.8 Sv) to the North Atlantic.

	1957	1981	1992	1998	2004	2010
Surface (>22.5 °C)						
Ekman	4.5	3.7	4.6	5.2	4.5	2.1
Florida Straits	11.4	11.4	11.1	12.5	11.7	11.2
Mid-Ocean	−5.4	−4.4	−3.2	−5.3	−0.5	−3.3
Total	10.5	10.7	12.5	12.4	15.7	10.1
Thermocline (12.5–22.5 °C)						
Florida Straits	14.9	14.9	14.6	16.2	15.2	14.7
Mid-Ocean	−11.8	−14.0	−13.0	−16.7	−22.5	−14.2
Total	3.1	0.9	1.6	−0.5	−7.3	0.5
Lower Thermocline (9.5–12.5 °C)						
Florida Straits	2.8	2.8	2.6	3.2	2.9	2.7
Mid-Ocean	−0.1	−0.4	−1.3	−1.1	−1.0	−0.6
Total	2.7	2.4	1.3	2.1	1.9	2.1
Upper layer total	16.3	14.0	15.4	14.0	10.4	12.6

	1957	1981	1992	1998	2004	2010
Intermediate (5–9.5 °C)						
Florida Straits	2.0	2.0	2.0	2.1	2.0	2.0
Mid-Ocean	3.1	2.0	−0.1	−0.8	1.9	0.8
Total	5.1	4.0	1.9	1.3	3.9	2.7
UNADW						
SLSW *(4–5 °C)*	−2.0	−2.1	−1.3	−2.8	−2.1	−3.4
LSW *(3.2–4 °C)*	−5.1	−3.3	−4.1	−5.1	−5.8	−7.1
ISOW *(2.5–3.2 °C)*	−6.1	−3.6	−4.2	−3.7	−2.6	−3.9
Total	−13.2	−9.0	−9.6	−11.6	−10.5	−14.4
LNADW						
DSOW *(1.8–2.5 °C)*	−12.6	−13.6	−9.8	−6.5	−6.3	−3.1
AABW (<1.8 °C)	3.6	3.7	1.4	2.0	1.8	1.4
Lower layer total	−17.1	−14.9	−16.1	−14.8	−11.1	−13.4

In the deep ocean, the partitioning of transport variability into potential temperature classes highlights some interesting changes. Transport variability in depth classes showed a possible compensating enhancement/reduction of southward UNADW/LNADW over time (Fig. 8). In potential temperature classes, Fig. 11 shows that such compensating changes may have occurred specifically in the LSW and DSOW, which show a monotonic enhancement/reduction in southward transport since the 1981 section, respectively. Despite occupying a relatively narrow depth range at 25° N, LSW (3.2–4 °C) shows a trend in transport not reflected by either the ISOW or SLSW surrounding it. DSOW (1.8–2.5 °C) is the only water mass comprising the LNADW (Table 3) and accounts for all the reduction in southward transport in this layer. In Fig. 11 it is clear that the reduction in southward DSOW transport from 1981–2010 of ≈10 Sv is not fully compensated by an increase in LSW transport from 1981–2010 of ≈4 Sv. As shown in Fig. 8 in depth classes, removal of a seasonal sampling bias acts to enhance transport trends in the UNADW by several Sverdrups (whilst the LNADW is relatively unaffected). Whilst it is not yet possible to partition this seasonal transport cycle into potential temperature classes, the seasonally adjusted trend in southward LSW transport is likely to be a few Sverdrups greater than that shown in Fig. 8, which will further compensate for the observed reduction in DSOW. It is likely that the SLSW and ISOW also suffer from a similar seasonal sampling bias, and that they also help compensate for reduced DSOW flow since 1981, however, at least half this compensation seems to occur within the LSW where a monotonic trend is observed.

If these transport changes are considered in finer potential temperature divisions (not shown), most of the DSOW transport changes occur in its coldest waters, <2.3 °C. Record low DSOW transport in the 2010 section is partly due to the absence of transport in waters colder than 1.9 °C, which results from the choice of 1.9 °C as the boundary between DSOW and AABW in 2010 (the warmest in all six sections). Although some southward flow occurred in the 2010 section at potential temperatures <1.9 °C, the choice of 1.9 °C still acts to maximise southward flow in the DSOW and, thus, the record-low transport in 2010 is a robust result. Most of the increase in southward LSW transport occurs in its colder waters, <3.8 °C.

Transport variability within the deeper water mass classes captures variability similar to that described for depth classes (Sect. 3.1.3) and, thus, can be susceptible to similar sub-seasonal transport variability, particularly approaching the western margin. However, the vertical structure of the transport changes revealed in the potential temperature classes implies some longer term variability may have occurred within water masses which are expected to be the chief communicators of high latitude buoyancy flux changes to the low latitudes.

3.3 Water mass changes and isopycnal heave in the DWBC

In the above analysis, it has been suggested that interannual or longer term transport changes that are several Sverdrups in magnitude may have occurred in the NADW at 25° N over the past 50 years. To complement this result, a brief analysis of concurrent NADW water mass changes in the DWBC is now presented. This concentrates on the DSOW (the LNADW) where the greatest reduction in transport was observed in the six hydrographic sections (Fig. 11).

Contour plots of salinity changes on climatological potential density surfaces for the six hydrographic sections are initially considered to illustrate the nature of water mass changes at 25° N. These are shown in Fig. 12 for the 1981 and 1998 sections relative to the 2010 section for both the upper and deep ocean. In the deep ocean, it is immediately apparent that on isopycnal surfaces the greatest changes in water mass properties have occurred west of ≈65° W approaching the western margin. In this region waters have freshened continuously on isopycnal surfaces by 0.01 to 0.02 over the past fifty years across the six hydrographic sections (though this result necessitates some caution given a salinity bias may exist in the 1957 dataset, as noted by Bryden et al., 1996, and highlighted in Sect. 2.1). These changes are particularly coherent within the DSOW at 3000–5000 m depth though fairly prominent as well within the depth range of the ISOW and LSW (1500–3000 m). At 26° N, southward DWBC flow is observed within ≈100 km of the ocean margin at depths greater than 1000 m (with a core located ≈50 km offshore flowing at ≈10–20 cm s^{-1}), whilst diffuse northward recirculation is observed extending eastward away from the western boundary for hundreds of kilometres (Chave et al., 1997; Bryden et al., 2005a; Johns et al., 2008). The structure of the salinity changes shown in Fig. 12 is, therefore, consistent with the well-established view that water masses formed in the high northern latitudes arrive at 26° N in the DWBC and recirculate in its associated gyre. This general circulation is also seen in the oxygen sections (Fig. 3) where the youngest, highly oxygenated waters occur in the DWBC and its recirculation-gyre, before spreading (mixing and ageing) slowly over time throughout the remainder of the basin.

Figure 13a shows θ-S properties averaged over the DWBC region 77° W–70° W for the UNADW and LNADW. It is clear that water mass changes have occurred throughout the NADW and as expected a more or less continuous freshening and cooling have occurred on potential density surfaces (σ_4) from 1957 to 2010, as described above. This is particularly evident in the DSOW and NAIW/ISOW (1.8–2.5 °C and 2.5–3.2 °C potential temperature ranges, respectively, Table 3) where a clear monotonic cooling and freshening on density surfaces is evident with time in the six hydrographic sections. In the LSW (3.2–4 °C) a broadly similar trend is apparent though this is no longer monotonic due to the intertwining of the 1981 and 1992 curves, and an apparent reversal of the recent cooling and freshening trend in the 2010 section (in LSW warmer than 3.5 °C). No θ-S trends are evident in the SLSW (4–5 °C) whose water mass properties vary more erratically over time. When overlaying θ-S curves from Rapid-WATCH observations in this region (Fig. 13b), several of the hydrographic θ-S curves fall outside the range of sub-seasonal and seasonal Rapid-WATCH variability, particularly in the DSOW, which is indicative of longer term trends. Rapid-WATCH variability is notably enhanced in the SLSW and LSW, diminishing in the ISOW and DSOW.

The Rapid-WATCH variability shown in Fig. 13 is calculated from the average of twice daily potential temperature and salinity profiles from moorings WB3 and WB5 (these are located at ≈76.5° W and 72° W, respectively, see Fig. 2). At each timestep, potential temperature and salinity profiles from WB3 and WB5 are averaged together on depth levels to provide a single set of profiles for each property from 2004–2009. The timeseries of a property at each depth level then has a linear trend removed. The resulting set of profiles are considered an estimate of sub-seasonal and seasonal θ-S variability averaged over the region 77° W–70° W. Mooring WB2 is not included when averaging as this is located within one eddy length scale of WB3 and would bias the average towards variability at the western margin and not the 77° W–70° W region as a whole.

Figure 13c–d shows potential temperature and salinity changes averaged over the depth range of the DSOW (3000–4700 m) on both depth (black lines) and potential density surfaces (red lines) for the six hydrographic sections relative to the 2010 section. A long term, decadal cooling and freshening trend is observed on depth surfaces which is outside

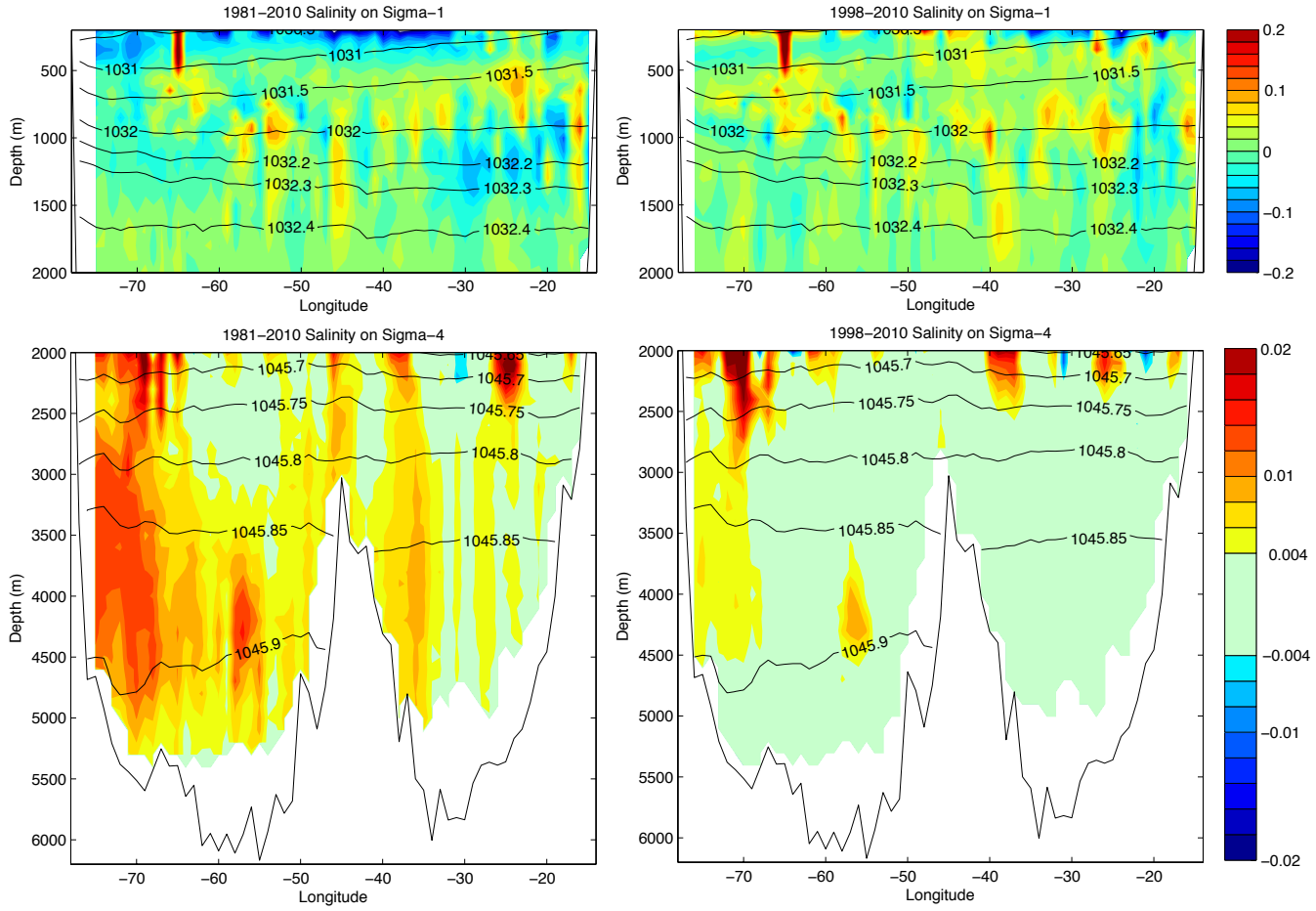

Fig. 12. Salinity changes on potential density surfaces across 25° N for the 1981 and 1998 hydrographic sections relative to the 2010 hydrographic section. Upper plots are for the upper ocean using σ_1 density surfaces (salinity contours are in 0.02 increments), lower plots are for the deep ocean using σ_4 density surfaces (salinity contours are in 0.002 increments, $\pm$0.004 denotes uncertainty). To facilitate comparison, each hydrographic section is bi-linearly interpolated onto a climatological potential density grids (σ_1 and σ_4) computed from the Hydrobase 2 database (a seasonally averaged hydrographic climatology, see http://www.whoi.edu/science/PO/hydrobase). This approach assumes property linearity in space and also linearity of the equation of state which is reasonable over small changes in potential density.

the range of Rapid-WATCH sub-seasonal and seasonal variability (black bars, estimated for the 77° W–70° W DWBC region as described above).

A common approach used to interpret potential temperature and salinity changes observed on depth surfaces is to decompose these changes into two components. The first is a density compensated change in water mass θ-S properties (which is the property change along isopycnal surfaces) and the second is property change along the historical θ-S curve associated with isopycnal heave. Cunningham and Alderson (2007) used this approach to decompose property changes in the 1957 to 2004 hydrographic sections (over 75° W–65° W). They showed that for DSOW, property changes from 1957 to 2004 on fixed pressure surfaces can be principally explained by property changes on isopycnal surfaces, though isopycnal heave accounts for $\approx$1/3 of the change in potential temperature. This decomposition approach assumes that water mass property changes (in this case DSOW) are density compensated (i.e., always change along isopycnal surfaces). However, some authors have suggested that water mass property changes may also be non-density-compensated (Bindoff and McDougall, 1994), evidence of which has been found in LSW at 26.5° N (Vaughan and Molinari, 1997). Figure 13c–d, however, supports the approach of Cunningham and Alderson (2007), showing that the potential temperature and salinity changes observed on depth levels in the DSOW (black lines) can be explained as the combination of a long-term density compensated cooling and freshening of the DSOW along isopycnal surfaces (red lines) and deviations from this long-term density compensated trend associated with isopycnal heave on sub-seasonal timescales (black bars). Here, the sub-seasonal property variability on depth surfaces observed by Rapid-WATCH (black bars) is taken to represent isopycnal heave which is dominant at these timescales.

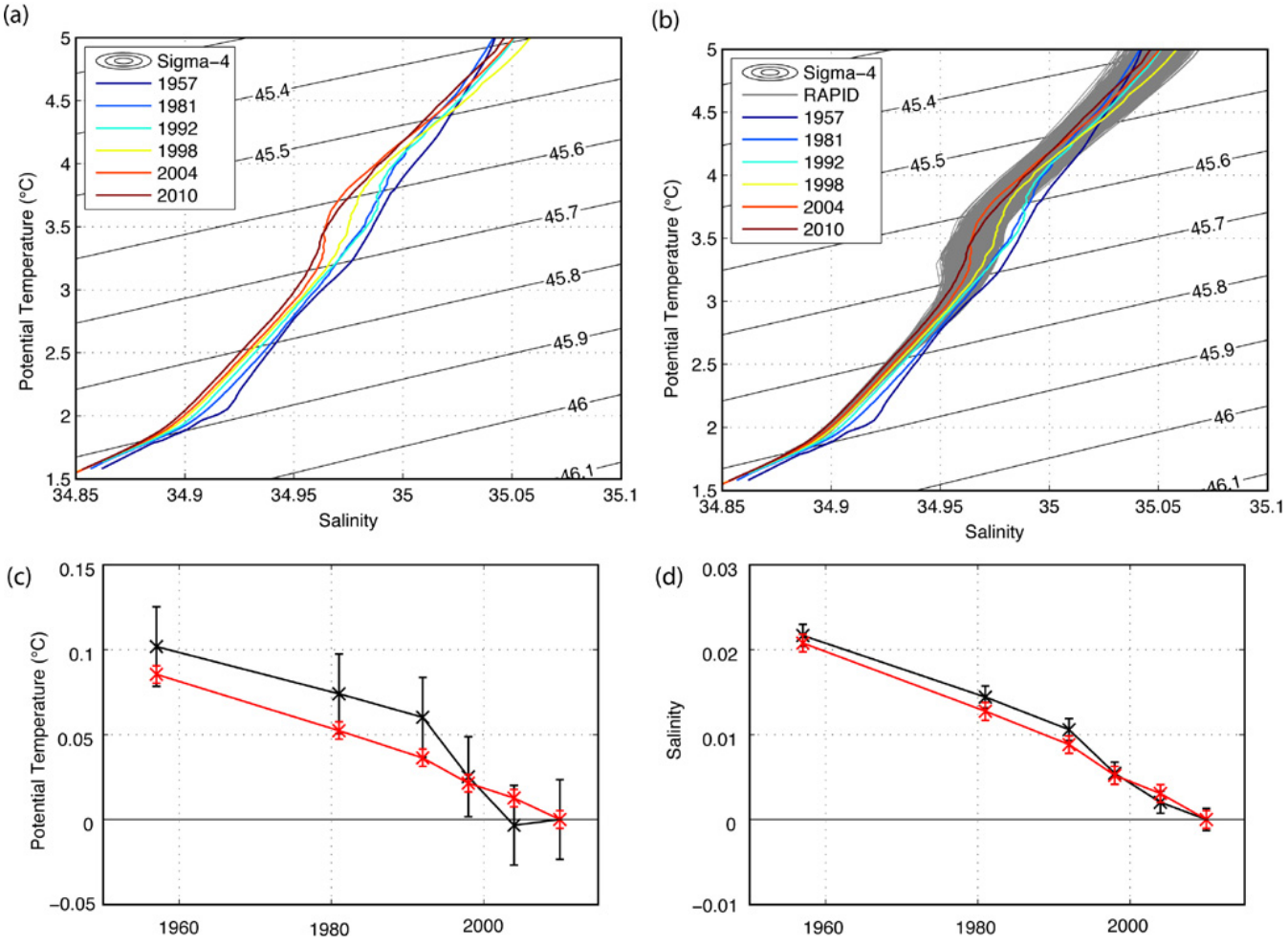

Fig. 13. Top (**a**–**b**), θ-S plots of water mass properties averaged over the longitudinal range 77° W–70° W for the six hydrographic sections in the the upper and lower North Atlantic Deep Waters **(a)**, and with all twice daily Rapid-WATCH profiles (2004–2009) overlaid **(b)**. The Rapid-WATCH profiles shown are the average of moorings WB3 and WB5 (see text). σ_4 potential density surfaces are shown. Bottom (**c**–**d**), potential temperature **(c)** and salinity **(d)** changes in the LNADW (3000–4700 m depth range) for the six hydrographic sections averaged over 77° W–70° W. Changes are shown relative to 2010. Black lines denote changes on depth surfaces and red lines denote changes on potential density surfaces (σ_4). Error-bars denote ± 1 std. dev. of property variability calculated from de-trended Rapid-WATCH mooring data (2004–2009, average of WB3 and WB5, see text).

The above results imply that long-term changes in DSOW properties have been (near) density compensated. Because density compensated water mass changes will not result in a change in isopycnal slope (and, hence, geostrophic transport) over time, this suggests that the interannual and longer term transport changes of several Sverdrups described for the DSOW in the previous Sections cannot be explained by changes in high latitude water mass properties which advect into the 25° N section along the DWBC. Instead, transport changes must be due to changes in isopycnal slope associated with some other dynamic process. This is explored below. It is emphasised that water mass changes that are not density compensated (i.e., water mass changes that have not taken place solely along isopycnal surfaces) or isopycnal heave on timescales longer than sub-seasonal cannot be ruled out in Fig. 13c–d, but these cannot be distinguished from short term variability.

Figure 14 shows that transport variability associated with property variability averaged across the DWBC does not account for long-term transport changes of several Sverdrups in the DSOW (see also Atkinson, 2011). The reduced LNADW (or DSOW) transport in 1998, 2004 and 2010 relative to the earlier 1957, 1981 and 1992 hydrographic sections is achieved noisily via a reduction in southward cumulative transports approaching the western basin margin, and not through any obvious structured reduction in cumulative transports across the DWBC and its recirculation gyre (Fig. 9 and Sect. 3.1.5). For the LNADW or UNADW the reduced or enhanced southward transport in the later hydrographic sections occurs due to a pronounced deepening or

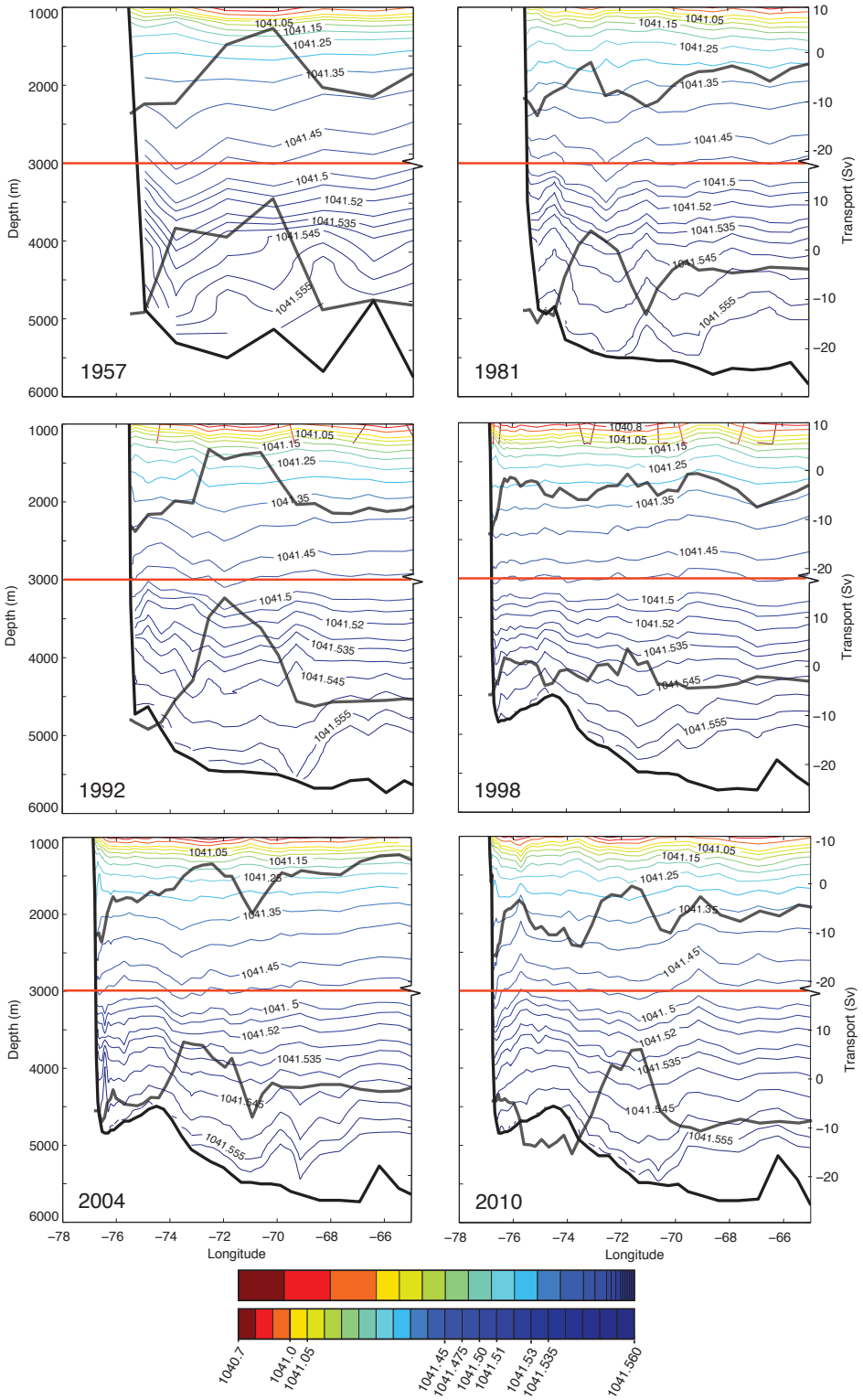

Fig. 14. Potential density (σ_3) contour plots in the deep ocean at the western Atlantic margin for the six hydrographic sections. Note the nonlinear scale of density contours (lower colourbar; contour separation reduces with increasing depth, from 0.1 to 0.05, 0.025, 0.01 and 0.005 kg m^{-3}). For emphasis, a linear colourbar is also included (upper colourbar). Overlain in grey are UNADW and LNADW cumulative transports from Fig. 9 (red horizontal line denotes the 3000 m depth interval used to separate UNADW and LNADW in this study).

shallowing of isopycnals below or above depths of around 2500 m (Fig. 14). This occurs within a few degrees of longitude (a few hundred kilometres) of the western margin and is particularly pronounced for the 2010 section. Below 2500 m, this isopycnal heave is associated with changes in isopycnal depth of several hundred metres.

Pronounced changes in the deep ocean density structure at the western margin between the later and earlier sections are seen in dynamic height anomaly profiles relative to 2010 close to the western margin for the six hydrographic sections (Fig. 15). A reduced shear in the dynamic height field between UNADW and LNADW layers in the recent versus earlier sections results in a reduction in LNADW transport (deeper than 3000 m) close to the western boundary. Isopycnal heave within a few hundred kilometres of the western margin, thus, appears to explain the reduction in LNADW transport in the 1998–2010 sections. This dynamic height variability at the western margin lies within the range of variability observed by Rapid-WATCH (Fig. 15). It is noted that whilst the 1957 data lies at the extreme of the Rapid-WATCH envelope, this is no longer the case if a possible salinity bias in the 1957 dataset (Sect. 2.1) is accounted for, which brings it more in line with the 1981 data.

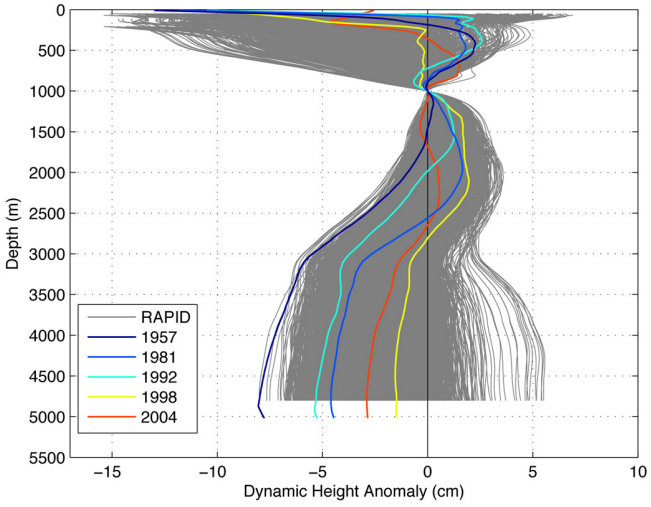

Fig. 15. Dynamic height anomaly profiles (cm) for the six hydrographic sections, with respect to the 2010 section (i.e., the dynamic height profile for the 2010 section is subtracted from all other profiles), for profiles adjacent to the western boundary. Dynamic height anomaly profiles from 5 years of Rapid-WATCH western margin mooring data are also shown. A reference level of 1000 m is assumed in the region of the DWBC, consistent with the calculation of transports described in Sect. 2.3. Each hydrographic dynamic height profile is constructed by merging together hydrographic stations adjacent to the western margin (e.g., if the western most station extends from the surface to 200 m depth, this is then merged with data deeper than 200 m from the next station east; this appending process is continued until a single full depth hydrographic profile is obtained reaching from the surface to 5000 m depth). For Rapid-WATCH data, WB2 data shallower than 4000 m are merged with WB3 data deeper than 4000 m (Sect. 2.2).

4 Discussion

This study suggests that NADW transport variability may have occurred that has a period longer than seasonal variability. It is not yet clear, however, whether this variability is interannual or decadal in timescale and at present the Rapid-WATCH timeseries is too short to assess the magnitude of interannual transport variability. Observations of deep water transport variability elsewhere in the North Atlantic that may help resolve this issue are sparse in both time and space and those observations that do exist at high latitudes are difficult to reconcile with transport variability in this study. Some studies have described decadal deep water transport variability in the DWBC of the Irminger Sea (Kieke and Rhein, 2006; Bacon, 1998; Sarafanov et al., 2009, 2010a) of order ±2–2.5 Sv, with minima in the 1950s and mid-1990s, maxima in the early 1980s and mid to high values in the 2000s, and which is coherent in the UNADW and LNADW. If anything a multi-decadal and anti-correlated variability in the LNADW and UNADW is described here at 25° N, with southward LNADW/UNADW transport stronger/weaker by a few Sverdrups in the 1960s to 1980s versus the 1990s to 2000s (Fig. 8). Interestingly, Sarafanov et al. (2009) also noted an anti-correlation between decadal DWBC transport variability in the Irminger Sea and the production of LSW (consistent with e.g. Koltermann et al., 1999; Marsh, 2000) which may be due to an opposing response to NAO forcing (Dickson et al., 1996), to changes in sub-polar gyre extension and strength (e.g. Bersch et al., 2007), or to blocking of ISOW flow through the Charlie-Gibbs Fracture Zone by enhanced LSW production, which could have arrived within a few years of formation (e.g. Kieke and Rhein, 2006). At the Greenland-Scotland overflows themselves, Hansen et al. (2001) concluded that there has been a 20 % reduction in baroclinic Faroe Bank overflow transport since 1950, however, Olsen et al. (2008) contested this finding, suggesting there was no significant trend in either Faroe Bank or total Greenland-Scotland ridge overflow transports into the North Atlantic for the period 1948–2005 (with variability amounting to ±1 Sv). Variability at the overflows is not necessarily correlated with downstream flow as the volume of water entrained at the overflows may vary.

South of the Irminger Sea, an increase in DWBC transport at ≈53° N in the Labrador Sea from 1996–2003 has been observed, consistent with increases observed in the Irminger Sea since the mid-1990s (Sarafanov et al., 2009). Increased transport in the 2000s was also found by Han et al. (2010) at 56° N, who implied a weak barotropic response to the NAO via wind stress curl. How the temporal evolution of LSW transport relates to total NADW transport and AMOC variability is not clear (Dengler et al., 2006). Hakkinen and

Rhines (2004) suggested declining sub-polar circulation in the 1990s is driven by buoyancy forcing, though this is challenged by modelling studies emphasising a role for wind-stress variability (Boening et al., 2006; Biastoch et al., 2008) and a recent intensification in circulation (Dengler et al., 2006; Sarafanov et al., 2010b) despite low net heat flux and weak deep convection in the Labrador Sea. Near the deep AMOC limb exit of the Labrador Sea, Fischer et al. (2010) found no trend in transport for the period 1997–2009 despite a warming trend of 0.05 °C yr^{-1}, consistent with Schott et al. (2006) who found a similar warming trend since 2001 in the DWBC LSW core at 43° N, but no change in DWBC transport east of the Grand Banks from 1993–2005. DWBC transport time series south of the Irminger Sea are somewhat short for assessing multi-decadal changes in NADW transport, but they do conflict with findings in this study of a monotonic increase/decrease in southward transport of LSW/DSOW at 25° N since 1981 and an increase in southward ISOW transport in the 2010 section.

At present it remains an open question whether, and at what timescales DWBC transport variability is coherent in the North Atlantic. The paradigm of the meridional overturning circulation operating like a simple conveyor belt is being challenged in modern studies (Lozier et al., 2010; Lozier, 2010).

Water mass changes in the DWBC at 25° N, briefly described in Sect. 3.3 for the six hydrographic sections, are consistent with changes observed at sub-polar latitudes. The cooling and freshening of DSOW at 25° N over more than half a century is consistent with observations of freshening DSOW at the Greenland-Scotland Ridge overflows and in the Labrador and Irminger Seas (e.g. Dickson et al., 2002; Curry et al., 2003; IPCC, 2007), though trends at 25° N are smaller in magnitude, likely due to mixing with other waters on the journey south. Furthermore, in the LSW at 25° N, the cessation of a cooling and freshening trend on isopycnals in the 2010 section (shown in Fig. 13a) is consistent with a warming and salinification of central Labrador Sea Water in the late-1990s (e.g. IPCC, 2007; Yashayaev, 2007) and a transit-time of ≈10 years to 26.5° N (Molinari et al., 1998). The density compensated nature of decadal DSOW changes demonstrated in this study suggests that transport changes of several Sverdrups that may have occurred in the DSOW at interannual and decadal timescales have come about not through advective mechanisms (e.g. Hawkins and Sutton, 2008), but through some other dynamic mechanism such as boundary wave processes (e.g. Johnson and Marshall, 2002; Koehl and Stammer, 2008; Zhang, 2010).

5 Conclusions

In this study, interannual and decadal changes in transport determined from six hydrographic sections spread over half a century at 25° N have been assessed in the context of five years of Rapid-WATCH observations at similar latitudes. The main findings are summarised below.

- In the 2010 hydrographic section, the AMOC showed a return in strength towards pre-2004 values of ≈17–18 Sv (albeit reduced by 1–2 Sv due to a weak northward Ekman transport associated with a strong negative phase of the North Atlantic Oscillation). This is consistent within uncertainty with the mean AMOC strength observed by Rapid-WATCH (2004–2009) and is due to a reduction in southward upper mid-ocean gyre transport relative to the 2004 section. The absence of a trend in southward upper-mid ocean transport, and in decadal timeseries of northward Ekman and Florida Straits transports, means that no significant trend in the strength of the AMOC's upper limb has been detected in the six hydrographic sections.

- Interannual and decadal transport variability at all depths at 25° N, as assessed using hydrographic "snapshots", is difficult to discern above sub-seasonal and seasonal variability, as quantified in zonally-integrated Rapid-WATCH observations and seen in the geostrophic velocity fields of the hydrographic sections themselves. Aliasing of the seasonal cycle accounts for much of the strengthening trend seen in southward upper-mid ocean transport prior to the 2010 section.

- In the deep ocean, where sub-seasonal transport variability is reduced, evidence of stronger southward transport of UNADW and weaker southward transport of LNADW of order several Sverdrups is observed in recent hydrographic sections relative to the 1957 and 1981 sections. This incorporates a seasonal correction derived from the Rapid-WATCH data, though a substantial reduction in LNADW transport in the late 1990s and 2000s is seen without this being applied. This apparent decadal variability lies within, but at the edge of, the ±2 std. dev. range of sub-seasonal variability observed by Rapid-WATCH.

- In potential temperature classes, a monotonic decrease in DSOW transport is observed in the 1981 section data onwards. This is partly compensated by a monotonic increase in LSW transport over the same period. The structure of the transport changes seen in potential temperature classes suggests that changes seen in UNADW and LNADW transport in depth classes may not simply result from the aliasing of shorter term variability and could be interannual or decadal in nature. Short-term transport variability in potential temperature classes cannot yet be assessed using Rapid-WATCH data.

- A cooling and freshening of the DSOW in the DWBC and its recirculation gyre over the past half century appears density compensated. Transport changes in the

LNADW over this period are the result of isopycnal heave close to the western basin margin and in the vicinity of the DWBC.

Acknowledgements. Data from the RAPID-WATCH MOC monitoring project are funded by the Natural Environment Research Council (NERC) and are freely available from www.noc.soton.ac.uk/rapidmoc. Florida Current cable and section data are made freely available on the Atlantic Oceanographic and Meteorological Laboratory web page (www.aoml.noaa.gov/phod/floridacurrent/) and are funded by the NOAA Office of Climate Observations. NOAA NCEP-NCAR reanalysis data are freely available via the IRI/LDEO Climate Data Library (http://iridl.ldeo.columbia.edu/). NOC v1.1 climatology data are freely available via the NOC/OOC website (http://www.noc.soton.ac.uk/noc_flux/noc1_1.php). Hydrobase 2 data were obtained freely from http://www.whoi.edu/science/PO/hydrobase. Rapid-WATCH timeseries with transport variability isolated in the mid-ocean and at the western and eastern Atlantic margins were kindly provided by Eleanor Frajka-Williams (National Oceanography Centre, Southampton, UK). NERC's strategic research programme Oceans 2025 supported the 2010 25° N transatlantic section.

H. L. Bryden, S. A. Cunningham and B. A. King thank NERC for ongoing support of their research efforts. C. P. Atkinson was supported by a NERC PhD studentship.

Edited by: W. Jenkins

References

Atkinson, C. P.: Variability of the Atlantic Meridional Overturning Circulation at 26° N, Ph.D. thesis, School of Ocean and Earth Science, University of Southampton, Southampton, UK, 293 pp., 2011.

Atkinson, C. P., Bryden, H. L., Hirschi, J. J-M., and Kanzow, T.: On the seasonal cycles and variability of Florida Straits, Ekman and Sverdrup transports at 26° N in the Atlantic Ocean, Ocean Sci., 6, 837–859, doi:10.5194/os-6-837-2010, 2010.

Bacon, S.: Decadal variability in the outflow from the Nordic seas to the deep Atlantic Ocean, Nature, 394, 871–874, 1998.

Baringer, M. and Molinari, R.: Atlantic Ocean baroclinic heat flux at 24-26° N, Geophys. Res. Lett., 26, 353–356, 1999.

Bersch, M., Yashayaev, I., and Koltermann, K. P.: Recent changes of the thermohaline circulation in the subpolar North Atlantic, Ocean Dynam., 57, 223–235, doi:10.1007/s10236-007-0104-7, 2007.

Biastoch, A., Boening, C. W., Getzlaff, J., Molines, J.-M., and Madec, G.: Causes of Interannual-Decadal Variability in the Meridional Overturning Circulation of the Mid-latitude North Atlantic Ocean, J. Climate, 21, 6599–6615, doi:10.1175/2008JCLI2404.1, 2008.

Bindoff, N. and McDougall, T.: Diagnosing climate-change and ocean ventilation using hydrographic data, J. Phys. Oceanogr., 24, 1137–1152, 1994.

Boening, C. W., Scheinert, M., Dengg, J., Biastoch, A., and Funk, A.: Decadal variability of subpolar gyre transport and its reverberation in the North Atlantic overturning, Geophys. Res. Lett., 33, L21501, doi:10.1029/2006GL026906, 2006.

Bryden, H., Griffiths, M., Lavin, A., Millard, R., Parrilla, G., and Smethie, W.: Decadal changes in water mass characteristics at 24° N in the subtropical North Atlantic Ocean, J. Climate, 9, 3162–3186, 1996.

Bryden, H. L., Johns, W. E., and Saunders, P. M.: Deep western boundary current east of Abaco: Mean structure and transport, J. Mar. Res., 63, 35–57, 2005a.

Bryden, H. L., Longworth, H. R., and Cunningham, S. A.: Slowing of the Atlantic Meridional Overturning Circulation at 25° N, Nature, 438, 655–657, doi:10.1038/nature04385, 2005b.

Bryden, H. L., Mujahid, A., Cunningham, S. A., and Kanzow, T.: Adjustment of the basin-scale circulation at 26° N to variations in Gulf Stream, deep western boundary current and Ekman transports as observed by the Rapid array, Ocean Sci., 5, 421–433, doi:10.5194/os-5-421-2009, 2009.

Chave, A., Luther, D., and Filloux, J.: Observations of the boundary current system at 26.5 degrees N in the subtropical North Atlantic ocean, J. Phys. Oceanogr., 27, 1827–1848, 1997.

Chidichimo, M. P., Kanzow, T., Cunningham, S. A., Johns, W. E., and Marotzke, J.: The contribution of eastern-boundary density variations to the Atlantic meridional overturning circulation at 26.5° N, Ocean Sci., 6, 475–490, doi:10.5194/os-6-475-2010, 2010.

Cunningham, S. A. and Alderson, S.: Transatlantic temperature and salinity changes at 24.5° N from 1957 to 2004, Geophys. Res. Lett., 34, L14606, doi:10.1029/2007GL029821, 2007.

Cunningham, S. A., Kanzow, T., Rayner, D., Baringer, M. O., Johns, W. E., Marotzke, J., Longworth, H. R., Grant, E. M., Hirschi, J. J. M., Beal, L. M., Meinen, C. S., and Bryden, H. L.: Temporal variability of the Atlantic Meridional Overturning Circulation at 26.5° N, Science, 317, 935–938, doi:10.1126/science.1141304, 2007.

Curry, R., Dickson, B., and Yashayaev, I.: A change in the freshwater balance of the Atlantic Ocean over the past four decades, Nature, 426, 826–829, doi:10.1038/nature02206, 2003.

Dengler, M., Fischer, J., Schott, F. A., and Zantopp, R.: Deep Labrador Current and its variability in 1996–2005, Geophys. Res. Lett., 33, L21506, doi:10.1029/2006GL026702, 2006.

Dickson, B., Yashayaev, I., Meincke, J., Turrell, B., Dye, S., and Holfort, J.: Rapid freshening of the deep North Atlantic Ocean over the past four decades, Nature, 416, 832–837, 2002.

Dickson, R., Lazier, J., Meincke, J., Rhines, P., and Swift, J.: Long-term coordinated changes in the convective activity of the North Atlantic, Prog. Oceanogr., 38, 241–295, 1996.

Eden, C. and Willebrand, J.: Mechanism of interannual to decadal variability of the North Atlantic circulation, J. Climate, 14, 2266–2280, 2001.

Fine, R.: Tracers, time scales, and the thermohaline circulation – the lower-limb in the North-Atlantic Ocean, Rev. Geophys., 33, 1353–1365, 1995.

Fischer, J., Visbeck, M., Zantopp, R., and Nunes, N.: Interannual to decadal variability of outflow from the Labrador Sea, Geophys. Res. Lett., 37, L24610, doi:10.1029/2010GL045321, 2010.

Frajka-Williams, E., Cunningham, S. A., Bryden, H. L., and King, B. A.: Variability of Antarctic bottom water at 24.5° N in the Atlantic, J. Geophys. Res., 116, C11026, doi:10.1029/2011JC007168, 2011.

Fuglister, F. C.: Atlantic Ocean Atlas of Temperature and Salinity Profiles and Data From the International Geophysical Year of 1957-1958, , 209 pp., Woods Hole Oceanogr. Inst., Woods Hole, Mass., 1960.

Ganachaud, A.: Error budget of inverse box models: The North Atlantic, J. Atmos. Ocean. Tech., 20, 1641–1655, 2003.

Hakkinen, S. and Rhines, P.: Decline of subpolar North Atlantic circulation during the 1990s, SCIENCE, 304, 555–559, 2004.

Hall, M. M. and Bryden, H. L.: Direct estimates and mechanisms of ocean heat transport, Deep-Sea Res. Pt. I, 29, 339–359, 1982.

Han, G., Ohashi, K., Chen, N., Myers, P. G., Nunes, N., and Fischer, J.: Decline and partial rebound of the Labrador Current 1993–2004: Monitoring ocean currents from altimetric and conductivity-temperature-depth data, J. Geophys. Res., 115, C12012, doi:10.1029/2009JC006091, 2010.

Hansen, B., Turrell, W., and Osterhus, S.: Decreasing overflow from the Nordic seas into the Atlantic Ocean through the Faroe Bank channel since 1950, Nature, 411, 927–930, 2001.

Hawkins, E. and Sutton, R.: Potential predictability of rapid changes in the Atlantic meridional overturning circulation, Geophys. Res. Lett., 35, L11603, doi:10.1029/2008GL034059, 2008.

IPCC: Climate Change 2007: The Physical Science Basis. Contribution of working group 1 to the fourth assessment report of the IPCC, Cambridge University Press, 2007.

Jayne, S. R. and Marotzke, J.: The dynamics of ocean heat transport variability, Rev. Geophys., 39, 385–411, 2001.

Johns, W. E., Beal, L. M., Baringer, M. O., Molina, J. R., Cunningham, S. A., Kanzow, T., and Rayner, D.: Variability of shallow and deep western boundary currents off the Bahamas during 2004-05: Results from the 26° N RAPID-MOC array, J. Phys. Oceanogr., 38, 605–623, doi:10.1175/2007JPO3791.1, 2008.

Johnson, H. L. and Marshall, D. P.: A theory for the surface Atlantic response to thermohaline variability, J. Phys. Oceanogr., 32, 1121–1132, 2002.

Josey, S. A., Kent, E. C., and Taylor, P. K.: Wind stress forcing of the ocean in the SOC climatology: Comparisons with the NCEP-NCAR, ECMWF, UWM/COADS, and Hellerman and Rosenstein Datasets, J. Phys. Oceanogr., 32, 1993–2019, 2002.

Kanzow, T., Cunningham, S. A., Rayner, D., Hirschi, J. J. M., Johns, W. E., Baringer, M. O., Bryden, H. L., Beal, L. M., Meinen, C. S., and Marotzke, J.: Observed flow compensation associated with the MOC at 26.5° N in the Atlantic, Science, 317, 938–941, doi:10.1126/science.1141293, 2007.

Kanzow, T., Cunningham, S. A., Johns, W. E., Hirschi, J. J. M., Marotzke, J., Baringer, M. O., Meinen, C. S., Chidichimo, M., Atkinson, C. P., Beal, L. M., Bryden, H. L., and Collins, J.: Seasonal variability of the Atlantic Meridional Overturning Circulation at 26.5° N, J. Climate, 23, 5678–5698, doi:10.1175/2010JCLI3389.1, 2010.

Kieke, D. and Rhein, M.: Variability of the overflow water transport in the western subpolar North Atlantic, 1950–97, J. Phys. Oceanogr., 36, 435–456, 2006.

Koehl, A. and Stammer, D.: Variability of the meridional overturning in the North Atlantic from the 50-year GECCO state estimation, J. Phys. Oceanogr., 38, 1913–1930, doi:10.1175/2008JPO3775.1, 2008.

Koltermann, K., Sokov, A., Tereschenkov, V., Dobroliubov, S., Lorbacher, K., and Sy, A.: Decadal changes in the thermohaline circulation of the North Atlantic, Deep-Sea Res. Pt. II, 46, 109–138, 1999.

Larsen, J. C.: Transport and heat-flux of the Florida Current at 27°N derived from cross-stream voltages and profiling data – Theory and observations, Philos. T. Roy. Soc. A, 338, 169–236, 1992.

Lavin, A., Bryden, H. L., and Parrilla, G.: Meridional transport and heat flux variations in the subtropical North Atlantic, The Global Ocean and Atmosphere System, 6, 269–293, 1998.

Leaman, K. D., Molinari, R. L., and Vertes, P. S.: Structure and variability of the Florida Current at 27° N: April 1982–July 1984, J. Phys. Oceanogr., 17, 565–583, 1987.

Longworth, H. R.: Constraining variability of the Atlantic Meridional Overturning Circulation at 25° N from historical observations, 1980-2005, Ph.D. thesis, School of Ocean and Earth Science, University of Southampton, Southampton, UK, 200 pp., 2007.

Lozier, M. S.: Deconstructing the conveyor belt, Science, 328, 1507–1511, doi:10.1126/science.1189250, 2010.

Lozier, M. S., Roussenov, V., Reed, M. S. C., and Williams, R. G.: Opposing decadal changes for the North Atlantic meridional overturning circulation, Nat. Geosci., 3, 728–734, doi:10.1038/NGEO947, 2010.

Marsh, R.: Recent variability of the North Atlantic thermohaline circulation inferred from surface heat and freshwater fluxes, J. Climate, 13, 3239–3260, 2000.

Meinen, C. S., Baringer, M. O., and Garcia, R. F.: Florida Current transport variability: an analysis of annual and longer-period signals, Deep-Sea Res. Pt. I, 57, 835–846, 2010.

Molinari, R., Fine, R., Wilson, W., Curry, R., Abell, J., and McCartney, M.: The arrival of recently formed Labrador Sea Water in the deep western boundary current at 26.5° N, Geophys. Res. Lett., 25, 2249–2252, 1998.

Olsen, S. M., Hansen, B., Quadfasel, D., and Osterhus, S.: Observed and modelled stability of overflow across the Greenland-Scotland ridge, Nature, 455, 519–U35, doi:10.1038/nature07302, 2008.

Parrilla, G., Lavin, A., Bryden, H., Garcia, M., and Millard, R.: Rising temperatures in the subtropical North-Atlantic Ocean over the past 35 years, Nature, 369, 48–51, 1994.

Pond, S. and Pickard, G. L.: Introductory Dynamical Oceanography, Butterworth-Heinemann, 2nd edn., 329 pp., 1983.

Roemmich, D. and Wunsch, C.: 2 Transatlantic sections: Meridional circulation and heat flux in the subtropical North Atlantic Ocean, Deep-Sea Res., 32, 619–664, 1985.

Sarafanov, A., Falina, A., Mercier, H., Lherminier, P., and Sokov, A.: Recent changes in the Greenland-Scotland overflow-derived water transport inferred from hydrographic observations in the southern Irminger Sea, Geophys. Res. Lett., 36, L13606, doi:10.1029/2009GL038385, 2009.

Sarafanov, A., Falina, A., Lherminier, P., Mercier, H., Sokov, A., and Gourcuff, C.: Assessing decadal changes in the Deep Western Boundary Current absolute transport southeast of Cape Farewell, Greenland, from hydrography and altimetry, J. Geophys. Res., 115, C11003, doi:10.1029/2009JC005811, 2010a.

Sarafanov, A., Mercier, H., Falina, A., Sokov, A., and Lherminier, P.: Cessation and partial reversal of deep water freshening in the northern North Atlantic: observation-based estimates and attribution, Tellus A, 62, 80–90, doi:10.1111/j.1600-0870.2009.00418.x, 2010b.

Schmitz, W. and McCartney, M.: On the North-Atlantic circulation, Rev. Geophys., 31, 29–49, 1993.

Schott, F. A., Fischer, J., Dengler, M., and Zantopp, R.: Variability of the Deep Western Boundary Current east of the Grand Banks, Geophys. Res. Lett., 33, L21S07, doi:10.1029/2006GL026563, 2006.

Shoosmith, D. R., Baringer, M. O., and Johns, W. E.: A continuous record of Florida Current temperature transport at 27° N, Geophys. Res. Lett., 32, L23603, doi:10.1029/2005GL024075, 2005.

Smith, W. H. F. and Sandwell, D. T.: Global seafloor topography from satellite altimetry and ship depth soundings, Science, 277, 1956–1962, doi:10.1126/science.277.5334.1956, 1997.

Stouffer, R. J., Yin, J., Gregory, J. M., Dixon, K. W., Spelman, M. J., Hurlin, W., Weaver, A. J., Eby, M., Flato, G. M., Hasumi, H., Hu, A., Jungclaus, J. H., Kamenkovich, I. V., Levermann, A., Montoya, M., Murakami, S., Nawrath, S., Oka, A., Peltier, W. R., Robitaille, D. Y., Sokolov, A., Vettoretti, G., and Weber, S. L.: Investigating the causes of the response of the thermohaline circulation to past and future climate changes, J. Climate, 19, 1365–1387, 2006.

Vaughan, S. and Molinari, R.: Temperature and salinity variability in the deep western boundary current, J. Phys. Oceanogr., 27, 749–761, 1997.

Vellinga, M. and Wood, R. A.: Global climatic impacts of a collapse of the Atlantic thermohaline circulation, Climatic Change, 54, 251–267, 2002.

Yashayaev, I.: Hydrographic changes in the Labrador Sea, 1960–2005, Prog. Oceanogr., 73, 242–276, doi:10.1016/j.pocean.2007.04.015, 2007.

Zhang, R.: Latitudinal dependence of Atlantic Meridional Overturning Circulation (AMOC) variations, Geophys. Res. Lett., 37, L16703, doi:10.1029/2010GL044474, 2010.